Biofuel Research Journal 46 (2025) 2412-2431

Biofuel Research Journal

Journal homepage: www.biofueljournal.com

Original Research Paper

Sustainable biokerosene from lipids using efficient ozone cracking

Junli Liu[1,2,*], Elena Robles Molina[1,2], Nathan S. Moiser[1,2,*]

[1] *Department of Agricultural and Biological Engineering, Purdue University, West Lafayette, IN 47907, United States.*

[2] *Laboratory of Renewable Resources Engineering, Purdue University, West Lafayette, IN 47907, United States.*

HIGHLIGHTS

- Biokerosene is suitable for environments with temperatures as low as -67 ºC.
- Yields of biokerosene (No. 1 and No.2) can reach approximately 1.3 kg/kg oil.
- Emission analysis showed that biokerosene can reduce NOx emissions by up to 40%.
- Biokerosene use can reduce CO_2 emissions by over 93%.
- The annual biokerosene production in the U.S. could reach 25 BGal.

GRAPHICAL ABSTRACT

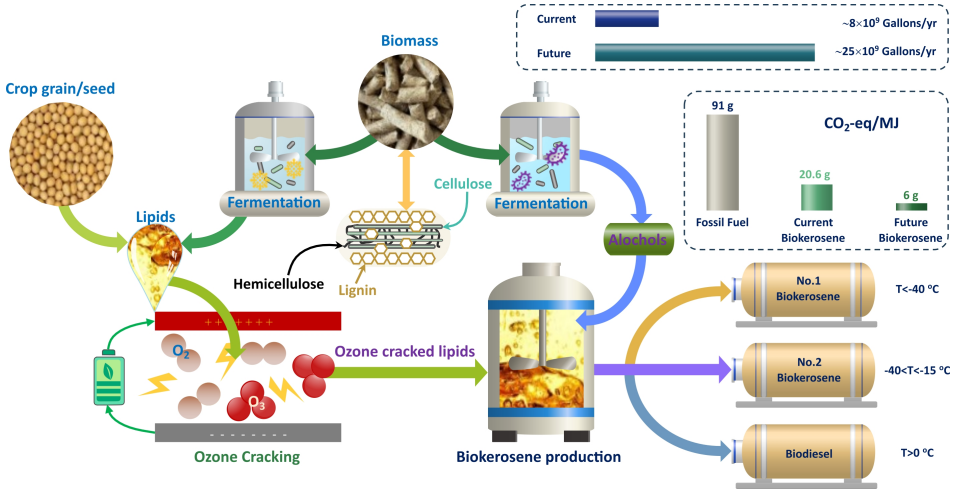

ARTICLE INFO

Article history:
Received 17 March 2025
Received in revised form 6 May 2025
Accepted 8 May 2025
Published 1 June 2025

Keywords:
Biokerosene
Ozone cracking
High oleic oils
Carbon sequestration
Combustion emissions
Sustainable aviation fuel

ABSTRACT

Diesel fuels and jet fuels will dominate the future liquid fuel market. Biodiesel, renewable diesel, and sustainable aviation fuel are alternatives for carbon sequestration in the transportation sector. However, biodiesel and renewable diesel are unsuitable for use during cold winter seasons or as jet fuel. Moreover, renewable diesel and sustainable aviation fuel face challenges such as harsh operating conditions and high energy consumption. A groundbreaking production process was investigated to synthesize biokerosene using nonanoic acid, a major compound from lipid ozone cracking. Various alcohols can be used to tune the physicochemical properties of biokerosene. The synthesized biokerosene exhibited excellent low-temperature performance, characterized by cloud points ranging from −35 to −67 °C, making it suitable for winter-season diesel, kerosene, and jet fuels. In addition, the products showed several superior qualities, such as long oxidation stability for extended storage, high flash points for safe handling, and high cetane numbers. Emission analysis indicated that the presence of oxygen in the fuel molecules facilitates combustion and reduces hydrocarbon and CO emissions. Moreover, nitrogen oxide emissions, associated with a global warming potential about 300 times that of CO_2, were significantly lower than those of biodiesel and jet fuel. Preliminary techno-economic analysis showed that the production cost of biokerosene was approximately USD 0.97/kg. Preliminary life cycle assessment showed CO_2 emissions of about 20.6 g CO_2-eq/MJ, representing a 77% reduction in greenhouse gas emissions. These emissions can be further reduced to about 6 g CO_2-eq/MJ with clean electricity and low-carbon alcohol. In summary, the biokerosene synthesis presented in this study offers a sustainable and economical route for producing winter-season diesel and jet fuel.

* Corresponding authors at:
E-mail address: liu18@purdue.edu (Junli Liu); mosiern@purdue.edu (Nathan S. Moiser)

Please cite this article as: Liu J., Molina E.R., Moiser N.S. Sustainable biokerosene from lipids using efficient ozone cracking. Biofuel Research Journal 46 (2025) 2412-2431. DOI: 10.18331/BRJ2025.12.2.4.

Contents

1. Introduction 2413
2. Materials and Methods 2414
2.1. Esterification of nonanoic acid with various alcohols 2414
2.2. Biodiesel production from soybean oil 2415
2.3. GC analysis of esters and nonanoic acid 2415
2.4. FTIR characterization 2415
2.5. Cloud point detection 2416
2.6. Density and viscosity 2416
2.7. Combustion heat 2416
2.8. Cetane number 2416
2.9. Oxidation stability 2416
2.10. Flashpoints 2416
2.11. Cold soak filtration test 2416
2.12. Boiling points 2416
2.13. TGA analysis 2416
2.14. Mass spectrum analysis 2416
2.15. Emission analysis 2416
3. Results and Discussion 2416
3.1. Synthesis of biokerosene from nonanoic acid with various alcohols 2416
3.2. Effect of types of FAEs on the biokerosene qualities 2417
3.3. Gas emission analysis of biokerosene and biokerosene/jet fuel blends 2420
3.4. Current and future biokerosene synthesis 2422
3.5. Challenges and perspectives on scale-up and commercialization 2424
3.6. Preliminary techno-economic analysis (TEA) and life cycle assessment (LCA) 2425
4. Conclusions 2429
Acknowledgments 2429
References 2429

Abbreviations

ASTM	American society for testing and materials	iPENE	isopentyl nonanoate
BGal	Billion gallons	iPNE	isopropyl nonanoate
BK	Biokerosene	LCA	Life cycle assessment
BNE	Butyl nonanoate	MMT	Million metric tons
DI	Deionized	MNE	Methyl nonanoate
DEAE	Diethyl azelate ester	MSA	Methane sulfonic acid
ENE	Ethyl nonanoate	NA	Nonanoic acid
FAE	Fatty acid ester	PNE	Propyl nonanoate
FAME	Fatty acid methyl ester	RD	Renewable diesel
FAEE	Fatty acid ethyl ester	SAF	Sustainable aviation fuel
FFA	Free fatty acid	TEA	Techno-economic analysis
GHG	Greenhouse gas	T_{onset}	Onset temperature
iBNE	isobutyl nonanoate	UHC	Unburned hydrocarbon

1. Introduction

Liquid hydrocarbons have been essential transportation fuels due to their high volumetric and gravimetric energy content. However, the combustion of fossil-based liquid hydrocarbons has led to increased atmospheric carbon dioxide (CO_2) concentrations and other environmental issues (Qu et al., 2020). Global warming, primarily driven by CO_2 emissions, caught international attention (Smith et al., 2019). Transportation fuels account for about 45% of total CO_2 emissions in the United States (U.S. EIA, 2023), and carbon sequestration through renewable feedstock-derived fuels is being used to mitigate climate change. With the electrification of passenger vehicles by 2035 in the United States, diesel and jet fuel are expected to become the dominant transportation fuels. Compared to hydrogen fuel, alcohols, and batteries, biodiesel, renewable diesel (RD), and sustainable aviation fuel (SAF) are currently promising alternatives due to their high energy density and compatibility with existing engines (**Fig. S1**). However, the feedstocks and synthesis routes for biodiesel, RD, and SAF vary significantly (**Figs. S2–S6**). RD and SAF can be synthesized from fats/oils, biomass, biomass-derived alcohols, or biomass-derived sugars, while biodiesel is derived solely from fats and oils.

Fats and oils, including free fatty acids (FFAs), have been commercially used to produce hydrocarbons through hydrogenation, yielding diesel fuels known as renewable or green diesel (Malins, 2021). However, the carbon chain lengths in RD typically range from 15 to 18, resulting in poor low-temperature performance and making it unsuitable for winter-season diesel or jet fuel. To address this, fats and oils are catalytically or thermally cracked to shorten the carbon chain length or isomerized to improve cold-flow properties (Wei et al., 2019). Nevertheless, the cost of converting oil to hydrocarbons strongly depends on the type of feedstock and varies widely. Fats and oils have also been extensively used in commercial biodiesel production over the past two decades, with FFA content significantly influencing production pathways. Compared to RD, biodiesel contains about 10% less energy but offers advantages such as higher cetane numbers and excellent engine lubricity. However, like RD, biodiesel also suffers from poor low-temperature performance due to the presence of saturated long-chain fatty acid esters (FAEs) (Liu and Tao, 2022a). Refining

Please cite this article as: Liu J., Molina E.R., Moiser N.S. Sustainable biokerosene from lipids using efficient ozone cracking. Biofuel Research Journal 46 (2025) 2412-2431. DOI: 10.18331/BRJ2025.12.2.4.

biodiesel through urea inclusion fractionation can efficiently remove saturated FAEs, thereby improving its low-temperature performance for winter-season diesel or jet fuel applications (Liu and Tao, 2022b; Liu et al., 2023b). The main challenges of this approach are reduced oxidation stability and increased nitrogen oxide emissions (Liu and Tao, 2022b; Liu et al., 2023b).

Biomass is another primary feedstock for hydrocarbons and can be converted into syngas, alcohols, and sugars for direct hydrocarbon synthesis (Liu et al., 2023c). Syngas, a mixture of carbon monoxide (CO) and hydrogen (H_2), is produced through biomass pyrolysis or gasification and can be converted to hydrocarbons *via* the Fischer–Tropsch process (Baliban et al., 2013; Voeten et al., 2024). However, the high capital investment required for large-scale operations to reduce production costs remains a major challenge (Diederichs et al., 2016). Additionally, the operating temperatures of the Fischer–Tropsch process significantly affect the composition of the resulting hydrocarbons. Syngas can also be converted into alcohols such as ethanol or butanediol through chemical synthesis or gas fermentation. The most common fermentation methods for producing alcohols, such as ethanol, n-butanol, and isobutanol, rely on starch or lignocellulosic sugars (Xue and Cheng, 2019; Fakayode et al., 2021; Mailaram and Maity, 2022; Liu et al., 2023a). Alcohols can also be derived from biomass pyrolysis (Bain et al., 2014; Chong and Ng, 2021). These alcohols are first dehydrated to form alkenes (e.g., ethylene or butene), which are then converted to hydrocarbons through oligomerization and hydrotreating (Wang et al., 2016; Kourkoumpas et al., 2024). The feasibility of the alcohol-to-hydrocarbon route depends on both alcohol and process costs and typically suffers from low carbon yields (Diederichs et al., 2016). Annual ethanol production in the United States is approximately 16 billion gallons (BGal) (Liu et al., 2023a), suggesting its potential as a feedstock for diesel or jet fuel pending further technological developments in fermentation and chemical synthesis, such as ultrasound-assisted purification (Naidu et al., 2021; Liu et al., 2023a). Biomass-derived sugars can also be used to synthesize hydrocarbons *via* direct hydrogenation (Davis et al., 2015), using intermediates such as farnesene, or through aqueous reforming with hydrotreating (Chong and Ng, 2021). The cost of converting sugars to hydrocarbons depends heavily on the specific pathway used (De Jong et al., 2014; Davis et al., 2015).

Table 1 presents a summary of selected technological pathways for producing jet fuel from different feedstocks, highlighting variations in yield, operating conditions, hydrogen consumption, production cost, and carbon intensity. The oil-to-jet fuel route offers high yields (~80%), whereas alternative pathways typically achieve lower yields (10–50%). Consequently, lower yields result in increased energy consumption during refining. Additionally, hydrogen consumption presents a major challenge across all current hydrocarbon synthesis routes, as renewable hydrogen remains expensive (IEA, 2021), and on-site hydrogen production can significantly increase capital costs (Diederichs et al., 2016). Meanwhile, the fractionation of biodiesel to biokerosene is limited by several drawbacks, including feedstock-dependent yields, reduced oxidation stability, and elevated nitrogen oxide emissions. Therefore, new routes are needed to address these limitations, such as converting oleic acid to biokerosene. Oleic acid is abundant in fats and oils (Liu and Tao, 2022a and b) and is especially concentrated in high oleic oils, such as high oleic soybean oil.

High oleic oils are new varieties characterized by high oleic acid content and low levels of saturated and polyunsaturated fatty acids. These oils were initially developed to improve oxidative stability and promote human health (Matlock, 2022), but they also offer promising industrial applications in biofuels and biochemicals (Nogales-Delgado et al., 2021; Orjuela et al., 2022). Additionally, oleic acid can be produced from lignocellulosic biomass *via* fermentation, providing a more sustainable source that does not compete with the food supply (Kruger et al., 2018). In this study, a new route to biokerosene was investigated using high oleic oil as the feedstock. Oleic acid was oxidized *via* ozone cracking to produce dicarboxylic and monocarboxylic acids with high yield. Specifically, ozone cracking of methyl oleate yields monomethyl azelate and nonanoic acid, demonstrating the feasibility of integrating this technology into biodiesel production.

While monomethyl azelate can serve as a monomer for biomaterials through polymerization, this study focused on biokerosene (nonanoate esters) synthesis *via* esterification of nonanoic acid with various alcohols, followed by fuel property characterization and emission analysis (**Fig. 1**). The resulting biokerosene exhibited excellent low-temperature performance and high oxidation stability. These enhanced qualities make it a strong candidate for use as winter-season diesel, kerosene, or aviation fuel. Compared to conventional biodiesel and RD, this biokerosene pathway offers high yields, low production costs, moderate operational conditions, valuable by-products, and consistent product quality. Furthermore, the use of renewable feedstocks contributes to carbon sequestration, enhancing the sustainability of the process.

2. Materials and Methods

2.1. Esterification of nonanoic acid with various alcohols

Esterification reactions were performed in a Soxhlet extraction system (24005-50, Kimble Kontes) with a 1 L flask. The flask was heated by a heating mantle with an adjustable voltage power supply (Superior Electric Co.), and the condenser of the Soxhlet extraction system was controlled by a refrigerated circulator (RTE-111, Thermo Scientific NES Lab, USA) at 1 °C. The alcohols used in this study included: methanol (≥ 99.9%, Sigma Aldrich Inc.), 200 proof ethanol (100%, Decon Laboratories Inc.), 1-propanol (≥ 99.9%, Sigma Aldrich Inc.), 2-propanol (≥ 99.9%, Sigma Aldrich Inc), 1-butanol (99.9%, Sigma Aldrich Inc.), isobutanol (≥ 99.9%, Supelco Inc.), and isopentanol (≥ 99.9%, Sigma Aldrich Inc.). Nonanoic acid (≥ 96%, Sigma Aldrich Inc.) reacted with alcohols to form esters using Methanesulfonic acid (MSA) (70%, Sigma Aldrich Inc.) as the homogeneous catalyst. In addition, 4 Å molecular sieves were used as the desiccant to remove the extra water generated during the reaction.

For a specific experiment, 0.7 moles of nonanoic acid, 4.2 moles of specific alcohol, and 0.014 moles of MSA (1.92 g of 70% MSA) were poured into the 1 L flask. 63 g of 4 Å molecular sieves were put into the

Table 1.
Summary of various routes to jet fuel.

Feedstock	Process Summary	Jet Fuel Yield (wt%)	Operations		Hydrogen Usage (g H_2/kg fuel)	MJSP (USD/gal)	CO_2 eq Emission (g CO_2/MJ)	Ref.
			T (°C)	P (Bar)				
Oils/fats	HEFA/HC*	40~77	200~475	10~300	~65.3	3.82~34.70	22.5~199	Diederichs et al. (2016); De Jong et al. (2017); Wei et al. (2019); Chong and Ng, (2021)
Ethanol	DOHD**	21~56	90~420	4~70	~12.1	3.65~10.91	26~78	Diederichs et al. (2016); Han et al. (2017); Chong and Ng, (2021)
Syngas[A]	FT***	7~19	180~350	20~40	~23.2	6.23~11.76	6~26	Diederichs et al. (2016); De Jong et al. (2017); Chong and Ng, (2021)
Sugar	DSHC****	~17	180~350	5~35	~50	7.17~24.42	15~93	De Jong et al. (2017); Chong and Ng, (2021); Walkling et al. (2025)
	APR*****	10~50	260~350	62~72	~12.1	4.66~12.00	56~58	Wang et al. (2016); Wei et al. (2019); Chong and Ng, (2021); Zoppi et al. (2023)

A: Gasification requires a temperature up to 1300 °C
* HEFA: Hydro-processed esters and fatty acids and HC: Hydrocracking
** DOHD: Dehydration, oligomerization, hydrogenation, and deoxygenation
*** FT: Fischer-Tropsch process
**** DSHC: Direct sugar to hydrocarbon
***** APR: Aqueous phase reforming

Please cite this article as: Liu J., Molina E.R., Moiser N.S. Sustainable biokerosene from lipids using efficient ozone cracking. Biofuel Research Journal 46 (2025) 2412-2431. DOI: 10.18331/BRJ2025.12.2.4.

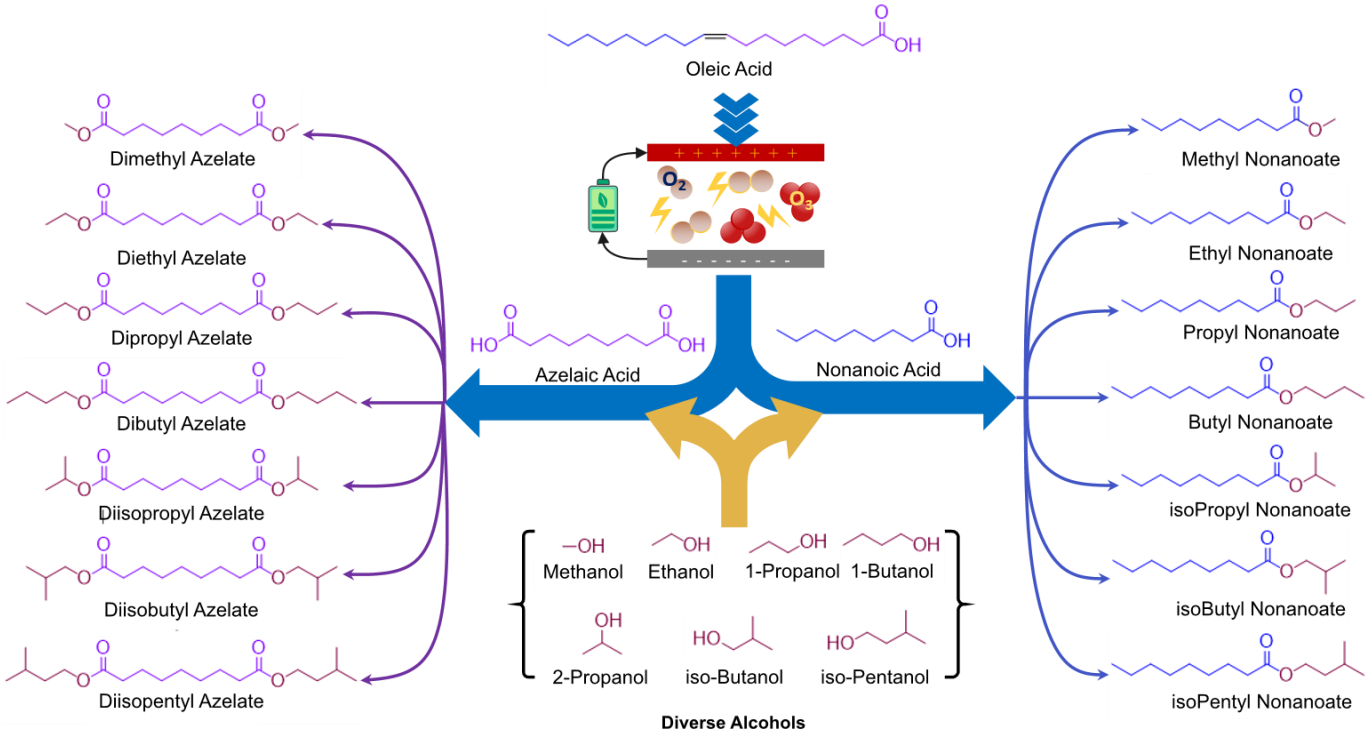

Fig. 1. Scheme of biokerosene (nonanoate/azelate) synthesis from oleic acid. Ozone cracking of oleic acid results in the carbon-carbon double bond cleavage to form azelaic and nonanoic acid. Nonanoic acid reacted with n-alcohol (such as methanol, ethanol, 1-propanol, and 1-butanol) and iso-alcohol (such as 2-propanol, isobutanol, and iso-pentanol) to form various nonanoate esters as biofuels or biochemicals. Azelaic acid reacted with n-alcohol (such as methanol, ethanol, 1-propanol, and 1-butanol) and iso-alcohol (such as iso-propanol, isobutanol, and iso-pentanol) to form various azelate esters as biokerosene.

thimble of the Soxhlet system. After the solution mixture was boiled for 6 h, the extra alcohol was evaporated by a Büchi R-200 rotary evaporator. Then, the residual mixture was poured into a 1 L separation funnel, and 100 mL of hexane and 200 mL of deionized (DI) water were added and vigorously mixed. The mixture was allowed to settle for 30 min before the bottom aqueous layers were drained. The previous hexane/water extraction step was repeated over 5 times until the aqueous layer became clear and the pH difference between the aqueous layer and DI water was less than 0.5. The top organic mixture was transferred to a 1 L flask, and hexane/water was removed to obtain the purified esters through evaporation using a Büchi R-200 Rotavapor. The purified esters were analyzed and characterized by various tests and analyses, such as FTIR, cloud point, freezing point, density, viscosity, and combustion heat.

2.2. Biodiesel production from soybean oil

Biodiesel production from soybean oil was carried out in a 2 L reactor. A heating mantle (USA Lab) equipped with a digital temperature controller was used to maintain the reaction temperature. To prevent methanol evaporation, a reflux condenser connected to a chiller bath (RTE-111, Thermo Scientific NES Lab, USA) was used to maintain the condenser temperature at 5 °C. A total of 900 g of soybean oil was transferred into the reactor and heated to approximately 50 °C. Then, 600 g of an MSA–methanol solution containing 3 wt% MSA was slowly added to the flask. Once the reaction mixture reached 68 °C, it was maintained at 68 ± 2 °C for 3 h.

The excess methanol was then removed using a Büchi R-200 rotary evaporator. The resulting mixture was transferred to a 2 L separation funnel and allowed to settle for at least 12 h before draining the bottom glycerol layer. The top layer was returned to the reactor, and 300 g of an MSA–methanol solution (3 wt% MSA) was added. The mixture was again heated to 68 °C and held for 3 h. After evaporating the excess methanol with the Büchi R-200, the remaining mixture was transferred to a separation funnel and allowed to settle for another 12 h. The bottom glycerol layer was drained, and 300 mL of hexane, along with 300 mL of deionized water, were added to the funnel. After vigorous shaking and 30 min of settling, the bottom aqueous layer was drained, and another 300 mL of DI water was added. This washing step was repeated until the pH difference between the aqueous layer and DI water was less than 0.5. Finally, the top organic layer was refined by removing residual hexane and water using the Büchi R-200 rotary evaporator.

2.3. GC analysis of esters and nonanoic acid

Samples were analyzed using a gas chromatograph (Agilent 7820A) equipped with a flame ionization detector (FID) and an autosampler/injector to determine esters and nonanoic acid. GC analysis was performed in a CP-Sil88 (Agilent Technologies) capillary column (50 m × 0.25 m × 0.2-μm). The detector and injector were set at 280° and 285°C, respectively. The CP-Sil88 analysis conditions were as follows: Column flow of 2.5 mL/min, helium carrier gas, 20:1 split ratio, and injection volume of 1 μL. The oven was programmed to 80°C and held for 2 min, then a programmed ramp to 120°C at 6°C/min and held for 1 min, then increased to 185°C at 10°C/min and held for 1 minute, finally heated to 225°C and held for 10 min.

2.4. FTIR characterization

FTIR analysis was performed by a Nicolet Nexus FTIR (Thermo Fisher Scientific, USA), and the samples were analyzed in a spectral region between 4000 and 800 cm^{-1} with a 2 cm^{-1} resolution. The samples for FTIR analysis included nonanoic acid, alcohols (methanol, ethanol, 1-propanol, 2-propanol, 1-butanol, isobutanol, and isopentanol), and esters formed by nonanoic acid with various alcohols.

Please cite this article as: Liu J., Molina E.R., Moiser N.S. Sustainable biokerosene from lipids using efficient ozone cracking. Biofuel Research Journal 46 (2025) 2412-2431. DOI: 10.18331/BRJ2025.12.2.4.

2.5. Cloud point detection

Cloud point was measured according to the ASTM D 2500. In the cloud point detection, a stainless-steel cylinder was immersed in the ethanol bath, and the temperature was chilled by adding dry ice. A glass test tube with about 25 mL of moisture-free sample was settled into the cylinder. The cloud point was recorded as the temperature at which waxy clouds or haze were observed.

2.6. Density and viscosity

The densities and viscosities of products were measured by a Stabinger viscometer (SVM 3001, Anton Paar) at -20 ºC, 15 ºC, and 40 ºC according to ASTM D 4052 and D 7042, respectively. Toluene was used as a solvent between injections to clean the system, and the instrument was calibrated and checked for accuracy using APS3 and APN2B Anton Paar-certified standards.

2.7. Combustion heat

Combustion heats of FAEs were detected and measured by a calorimeter (Isoperibol 6200, Anton Paar) with a water handling system according to ASTM D 4809. The combustion heat was measured by burning the equivalent mass of 0.7 mL of each sample in a bomb calorimeter filled with pure oxygen at 450 psi. The increment in the temperature of the water surrounding the bomb after ignition and complete combustion was automatically correlated, corrected, and reported by the system.

2.8. Cetane number

Cetane numbers were measured according to ASTM D 613 by the Southwest Research Institute. The sample was first used to rinse the engine tank and fuel line. The fuel flow rate was set to 13 mL/min, and the injection-timing micrometer of the fuel pump assembly was adjusted to achieve a $13.0° \pm 0.2°$ injection advance reading. The handwheel was then adjusted to vary the compression ratio and obtain a $13.0° \pm 0.2°$ ignition delay reading. It was essential to maintain stable injection advance and ignition delay readings. After verifying performance with the second reference fuel blend, the procedure was repeated with Reference Fuel No. 1, the sample, and then Reference Fuel No. 2. For each fuel, all parameters were checked carefully, and the system was allowed to reach equilibrium before recording the handwheel readings. The cetane number was calculated according to **Equation 1**.

$$CN_s = CN_{LRF} + (CN_{HRF} - CN_{LRF})(HW_s - HW_{LRF})/(HW_{HRF} - HW_{LRF}) \quad \text{Eq. 1}$$

where,
CN_S: cetane number of the sample,
CN_{LRF}: cetane number of low reference fuel,
CN_{HRF}: cetane number of high reference fuel,
HW_S: handwheel reading of sample,
HW_{LRF}: handwheel reading of low reference fuel,
HW_{HRF}: handwheel reading of high reference fuel.

2.9. Oxidation stability

Iowa Central Fuel Testing Laboratory, a BQ-9000 certified fuel testing laboratory, performed the oxidation stability according to EN 15751. The testing procedure was briefly described as follows: 10 L/h of purified air was induced into the biodiesel sample at 110 °C. The air carried the volatile organics from the oxidation to the container with distilled water. The conductivity of the water solution was continuously recorded, and the oxidation stability in hours was recorded when the conductivity rapidly changed.

2.10. Flashpoints

Flashpoints were measured according to ASTM D 93 using a Pensky-Marten closed cup tester. 70 mL of the sample was transferred to the testing cup. Once the fuel temperature reached about 20 ºC below the expected flashpoint, the ignition source was directed into the testing cup until the detection of a flash.

2.11. Cold soak filtration test

The cold soak filtration tests were performed according to ASTM D 7501. Biodiesel or biokerosene was warmed without heating to room temperature after being stored at 4±0.5 °C for 16 h. Then, 300 mL of biodiesel or biokerosene was filtered through a 0.7 μm glass fiber filter under a vacuum of 21 to 25 in Hg. The filtration time was recorded, and the allowed maximum filtration time was 360 seconds.

2.12. Boiling points

A 100 mL sample was poured into a 250 mL two-neck flask and heated with a heating mantle. A type K thermometer was put into the liquid without touching the glass. One neck was open to keep the pressure at 1 atm. When the liquid started boiling, the temperature was recorded, and the boiling point was the temperature without significant changing for 1 h.

2.13. TGA analysis

A TGA 4000 (Perkin Elmer, USA) was used to assess the thermal degradation by weight loss using nonisothermal and isothermal methods under a nitrogen atmosphere (20 mL/min). Nonisothermal heating was used to determine the T_{onset} of chemicals (esters and nonanoic acid) with 15-25 mg at 5 °C/min from 50 to 400 °C. T_{onset} was calculated by the tangent intersection of the baseline and degradation curve. The tangent intersection method was performed within the Origin software.

2.14. Mass spectrum analysis

The Thermo Finnigan LTQ Orbitrap mass spectrometer was used to detect positively charged ions generated with an atmospheric pressure chemical ionization (APCI) probe. The discharge voltage was 4.2 kV, and nitrogen as the sheath gas was set to an arbitrary flow rate of 50. Calibration of the instrument was performed using a standard Orbitrap calibration mixture, Pierce LTQ ESI Positive Ion Calibration Solution (#88322, ThermoFisher Scientific).

2.15. Emission analysis

Emission tests were performed using a 4-cycle air-cooled diesel engine (Yanmar L70N). Fuels, including biokerosene, biodiesel, jet fuel, and blends of biokerosene and jet fuel, were directly injected into the engine. The engine has a maximum rotation speed of 3600 RPM and a maximum power output of 4.9 kW. The engine was operated at about 50% engine load. The surrounding temperature was about 20 ºC. The exhaust gases were measured by an emission gas analyzer (Infrared Industries FGA 4000XDS exhaust gas analyzer) to analyze the concentrations of Unburned hydrocarbons (UHCs), CO, CO_2, and nitrogen oxides (NO_x).

3. Results and Discussion

3.1. Synthesis of biokerosene from nonanoic acid with various alcohols

Biokerosene synthesis from nonanoic acid with various alcohols was carried out, and the resulting esters could be used as fuels in diesel engines. Mass spectrum analysis of nonanoic acid and its derived esters in the range of m/z from 100 to 250 showed that the strongest signals varied significantly (**Fig. 2a**), and mass spectra with the range of m/z from 100 to 600 were shown in from **Figures S7** to **S14**. NA and Methyl nonanoate (MNE) had the strongest signal at m/z of 173.15, corresponding to $CH_3(CH_2)_7COOCH_4^+$. In contrast, all other esters (except Ethyl nonanoate (ENE)) had the strongest signal at m/z of 159.14, corresponding to $CH_3(CH_2)_7COOH_2^+$. ENE had two strong signals: one occurred at m/z of 159.14, corresponding to $CH_3(CH2)_7COOH_2^+$, and another one occurred at m/z of 187.17, corresponding to $CH_3(CH2)_7COOCH_2CH_4^+$. The peak at 1705.6 cm^{-1} in the FTIR spectrum of nonanoic acid corresponds to the carbonyl group (C=O) in carboxylic acid, and it disappeared in the synthesized esters. However, a peak appeared in the wavenumber of

Please cite this article as: Liu J., Molina E.R., Moiser N.S. Sustainable biokerosene from lipids using efficient ozone cracking. Biofuel Research Journal 46 (2025) 2412-2431. DOI: 10.18331/BRJ2025.12.2.4.

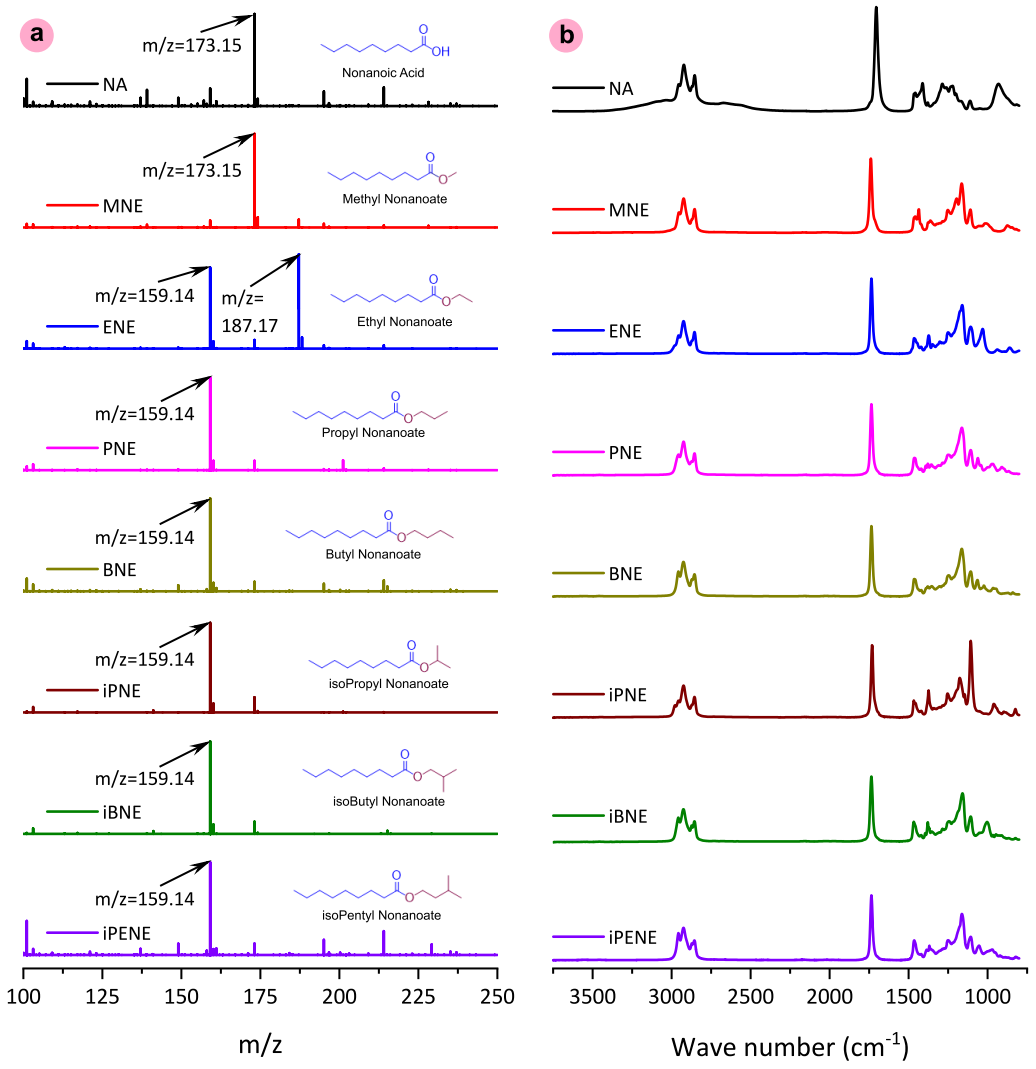

Fig. 2. Characterization of reactions: **(a)** mass spectrum of Nonanoic acid (NA) and synthesized esters; and **(b)** FTIR spectrum of NA and synthesized esters.

1735.7 cm^{-1} corresponding to the carbonyl group (C=O) in esters, indicating the ester formation after the reactions (**Fig. 2b**). The peak at 1165.7 cm^{-1} shows C–O stretching in the esters and the peak at 1225.5 cm^{-1} shows C–O stretching in carboxylic acids. The peak at 1165.7 cm^{-1} appeared in the FTIR spectra of all synthesized esters but was absent in that of nonanoic acid. Conversely, the peak at 1225.5 cm^{-1} appeared in the FTIR spectrum of nonanoic acid but disappeared in all synthesized esters. The broad peak from 2500 to 3500 cm^{-1} in the FTIR spectrum of nonanoic acid corresponding to the O–H in carboxylic group stretching (**Fig. 2b**) disappeared in the synthesized esters, the peak at 933.3 cm^{-1} in the FTIR spectrum of nonanoic acid corresponding to the O–H in carboxylic group bending (**Fig. 2b**) disappeared in the synthesized esters. All these phenomena of FTIR spectrum change indicated the replacement of the OH group in nonanoic acid by alkyl groups in esters after esterification reactions.

The esterification process of nonanoic acid with ethanol was analyzed using FTIR and gas chromatography (GC) analysis in **Figures 3a** and **3b**. According to FTIR analysis, the intensity of the carbonyl group in nonanoic acid at the wavenumber of 1705.6 cm^{-1} decreased with reaction time, but the intensity of the carbonyl group in ENE at the wavenumber of 1735.7 cm^{-1} increased with reaction time. According to GC analysis, the nonanoic acid peak at the residence time of 16 min decreased with reaction time, while the ENE peak at the residence time of 8.9 min increased with reaction time. However, the signal of nonanoic acid significantly reduced after 80 min of reaction for both FTIR analysis and GC analysis. These phenomena indicated that the esterification reaction approximately reached equilibrium. The synthesis of most esters exhibited a rapid reaction phase within the first 80 min, followed by a gradual approach to equilibrium, as shown in **Figure 3c**. However, isopropyl nonanoate (iPNE) synthesis demonstrated a slower reaction rate compared to the others, as shown in **Figure 3d**. In addition, utilizing molecular sieves to remove water can move the reaction direction to the esters to improve the yields of esters in **Figures 3c** and **3d** and **Table 2**. The yield of ester can reach over 0.999 after the second stage reaction (**Table 2**). The GC analysis of ester synthesis over time for the first stage reaction is shown in **Figs. S15-S30**.

3.2. Effect of types of FAEs on the biokerosene qualities

Low-temperature performance is the major challenge for current biodiesel to be used as winter-season diesel or aviation fuels (Liu and Tao, 2022b; Liu et al., 2023b). Cloud point appropriately characterizes the low-temperature performance based on the thermodynamic phase change (Liu and Tao, 2022a). Cloud points of current biodiesel range from -3 to 23 ºC, depending on the feedstock (Liu and Tao, 2022b), indicating inappropriate usage as winter-season diesel or jet fuel. The cloud points of # 2 winter season diesel for North America range from -7 to -28 ºC (Nowatzki et al., 2019), and the freezing point of aviation fuel is -40 ºC (ASTM D 7566,

Please cite this article as: Liu J., Molina E.R., Moiser N.S. Sustainable biokerosene from lipids using efficient ozone cracking. Biofuel Research Journal 46 (2025) 2412-2431. DOI: 10.18331/BRJ2025.12.2.4.

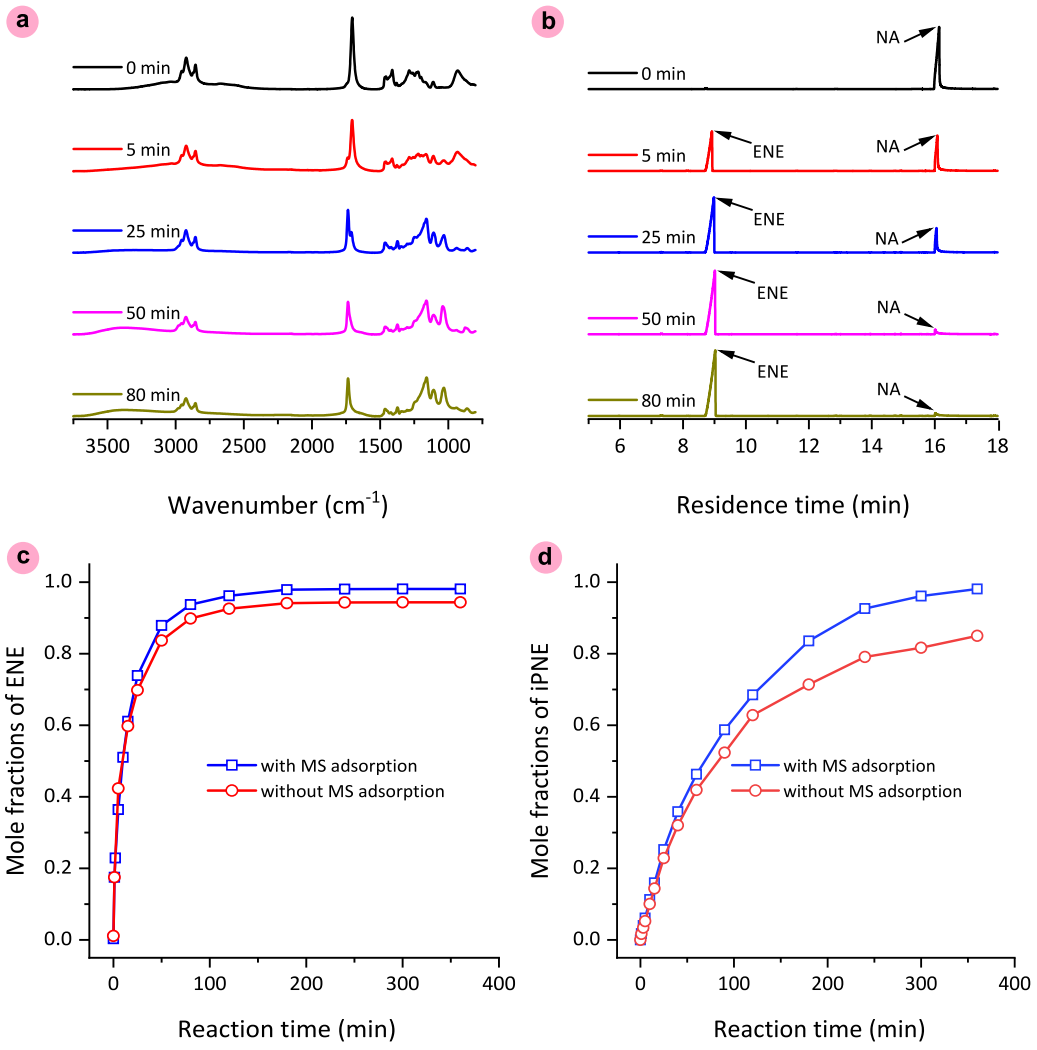

Fig. 3. Esterification process analysis: **(a)** FTIR spectrum of ENE synthesis with time; **(b)** GC signals of ENE synthesis with time; **(c)** yield of ENE synthesis over time; and **(d)** yield of isopropyl nonanoate (iPNE) synthesis over time.

Table 2.
Yields of esterification of nonanoic acid after the 1st stage reaction and the 2nd stage reaction.

Alcohol in the Esterification	1st Stage after 360 min		2nd Stage after 360 min	
	With MS	Without MS	With MS	Without MS
Methanol	0.986±0.011	0.980±0.009	>0.999	>0.999
Ethanol	0.984±0.009	0.952±0.015	>0.999	>0.999
1-propanol	0.995±0.008	0.978±0.010	>0.999	>0.999
1-butanol	0.989±0.010	0.974±0.011	>0.999	>0.999
Iso-propanol	0.976±0.013	0.797±0.021	>0.999	>0.999
Iso-butanol	0.981±0.011	0.971±0.009	>0.999	>0.999
Iso-pentanol	0.983±0.008	0.969±0.012	>0.999	>0.999

2022). Therefore, it is necessary to develop renewable alternatives to fossil-based winter-season diesel or jet fuel, such as biokerosene. According to the storage of 72 h under various temperatures (Fig. 4a), all fuel samples remained liquid at these temperatures except MNE at -40 ºC storage. The measured cloud points of biokerosene formed by nonanoic acid and various alcohols ranged from – 35 to – 67 ºC, depending on the type of alcohol used in synthesis (Fig. 4b). Because biokerosene has short carbon chain lengths (9 in carboxylic acid) compared to biodiesel (16 or 18) and diesel fuel (15 to 18), biokerosene can lower melting points to provide better low-temperature performance.

For linear molecules, the Van der Waals force and hydrogen bonds significantly increase with carbon chain lengths and can form more stable and ordered crystal structures. Consequently, molecules with short carbon chain lengths have lower melting points. However, the nonlinearity (e.g., isomerization and carbon-carbon double bond) of the structure can cause the reduced Van der Waals force and hydrogen bonds to lead the molecules to depart from the stable and ordered structure. Thus, the melting points decreased. Previous studies (Liu and Tao, 2022a and b) have shown that the increased nonlinearity for methyl esters with 18 carbon chain length caused the decreased melting points: methyl stearate (0 C=C, 38 ºC) > methyl oleate (1 C=C, -20ºC) > methyl linoleate (2 C=C, -35 ºC) > methyl linolenate (3 C=C, -52 ºC). Using iso-alcohol can cause branching in the ester tails, which provides reduced Van der Waals forces and hydrogen bonds. Consequently, the melting points of esters synthesized using iso-alcohols decreased.

Please cite this article as: Liu J., Molina E.R., Moiser N.S. Sustainable biokerosene from lipids using efficient ozone cracking. Biofuel Research Journal 46 (2025) 2412-2431. DOI: 10.18331/BRJ2025.12.2.4.

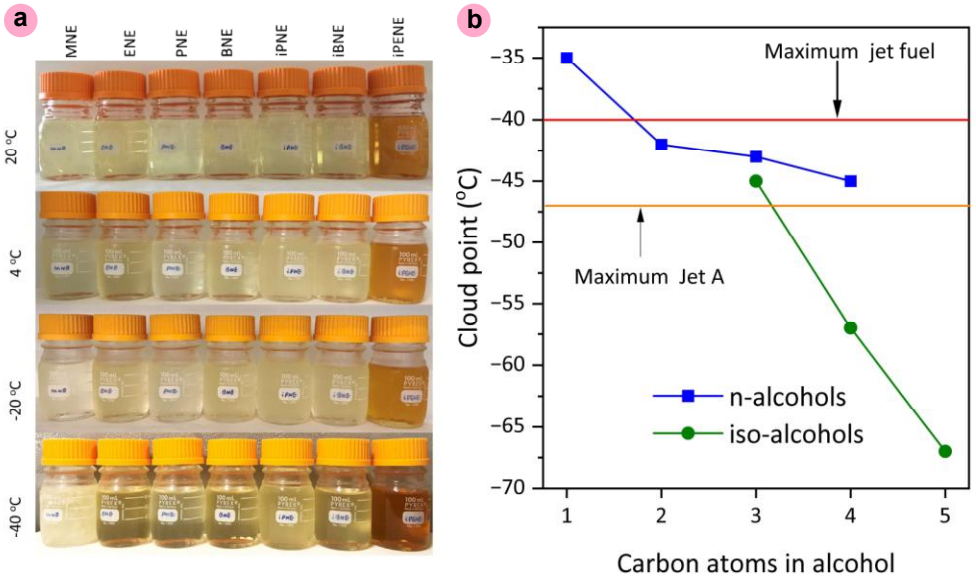

Fig. 4. Low-temperature performance of biokerosene: **(a)** biokerosene storage under various temperatures for over 72 h; and **(b)** measured cloud points of synthesized biokerosene.

For biokerosene synthesized with n-alcohols, the cloud points decreased significantly from MNE to ENE, while they slightly decreased for propyl nonanoate (PNE) and butyl nonanoate (BNE) compared to ENE (**Fig. 4b**). For biokerosene synthesized with iso-alcohols, the cloud points significantly decreased from iPNE to isobutyl nonanoate (iBNE) and isopentyl nonanoate (iPENE). Biokerosene synthesized with iso-alcohols resulted in lower cloud points because the alcohol isomerization resulted in less effective intermolecular packing to pack them together in the crystallization process. The effect of alkyl isomerization is more significant than hydroxyl isomerization to improve the low-temperature performance (**Fig. 4b**). The biokerosene samples have much better cold flow properties than winter season #2 diesel and current biodiesel from various feedstocks with cloud points ranging from -5 to 23 °C (Liu and Tao, 2022a and b; Liu et al., 2023b).

In addition to low-temperature performance, some other critical properties that influenced the synthesized biokerosene used as winter-season diesel or aviation fuel were also measured. Trucks and flights use diesel engines, which use compression ignition. It is crucial to determine whether the synthesized biokerosene can be used in diesel engines without damaging them. The cetane number, a crucial property of diesel fuel, indicates the ignition delay in diesel engines, with a minimum acceptable value of 40. The larger the cetane number, the shorter the ignition delay and the more complete the fuel combustion. The cetane numbers of the synthesized biokerosene were greater than 40 (**Fig. 5a**), indicating the appropriate use in diesel engines without damaging the engines. Moreover, cetane numbers increased with the carbon-chain length of the alcohol and were impaired by the alcohol isomerization (**Fig. 5a**). Since the carbon-carbon double bonds impair the cetane number and most biodiesel contains 60 to 90% of unsaturated components, the synthesized fully saturated biokerosene exhibited comparable cetane numbers to current biodiesel, even though the current biodiesel had a longer carbon-chain length (Liu and Tao, 2022a and b; Liu et al., 2023b).

Since diesel engines use compression ignition, fuel physical properties, such as viscosity, affect the atomization of fuel and droplet size in the combustion chamber (Shin et al., 2020). Moreover, too high viscosity results in incomplete combustion, large-sized soot formation, high greenhouse gas (GHG) emissions, and pump damage, but too low viscosity causes a lack of lubricity (Tat and Van Gerpen, 1999). The kinematic viscosities of synthesized biokerosene at 40 °C ranged from 1.4 to 2.3 mm^2/s, within the range of #1 diesel (1.3-2.4 mm^2/s). MNE's viscosities are close to ENE's at test temperatures (**Fig. 5b**), but the viscosities increased approximately linearly with carbon atoms in the alcohol used to synthesize the biokerosene. In addition, viscosities decreased with increasing temperature due to the higher rate of molecular motion and reduced cohesive forces, while the isomerization of alcohols used in the synthesis did not significantly affect the viscosities of the resulting biokerosene (**Fig. 5b**). In addition, jet fuel requires kinematic viscosities at – 20 °C less than 8 mm^2/s (ASTM D 7566, 2022), which made BNE, iBNE, and iPENE inappropriate for purely use in jet engines and recommended that they need to be blended with hydrocarbon jet fuel to reduce their viscosities.

Density is also an important property that inversely affects fuel atomization and volumetric energy density and inversely decreases with temperature (**Fig. 6a**). The gravimetric energy density of the synthesized biokerosene ranged from 35.5 to 38.1 MJ/kg, depending on the carbon atoms in alcohol molecules (**Fig. 5d**). The measured energy densities were less than the typical gravimetric energy densities of biodiesel (38 MJ/kg) and diesel fuels (43 MJ/kg) because of the short carbon-chain length and the existence of oxygen atoms. Volumetric energy densities were calculated according to the gravimetric energy density and the density at 15 °C (**Figs. 5c** and **5d**). The volumetric density of the synthesized biokerosene ranged from 31.3 to 33.3 MJ/L, influenced by the types of alcohol (**Fig. 5c**). Most of these calculated values were no more than the typical volumetric energy densities of biodiesel (33 MJ/kg) and diesel fuels (35-36 MJ/L). The energy is about 3 to 9% less than hydrocarbon diesel fuel, while the fuel weight is about 7% to 10% greater than the hydrocarbon fuel (**Figs. S31** and **S32**), depending on the type of synthesized biokerosene. These factors indicated the expected reduced mileage when using biokerosene.

Flashpoint is a critical specification for fuel storage and handling. Fuel with a flash point below 60 °C is classified as flammable, but fuel with a flash point above 60 °C is classified as combustible. Therefore, the biokerosene produced in this study is classified as combustible (**Fig. 6b**) because the measured flash points and published flash points (TGSC information system) ranged from 75 to 120 °C. As the number of carbon atoms in the alcohol increased, the flash point reached a minimum for ENE, then rose. The biokerosene synthesized from n-alcohols generally had flashpoints about 5 °C above biokerosene synthesized from iso-alcohols with the same carbon atoms. The difference in flash points among the biokerosene synthesized from alcohol isomers is caused by the difference in boiling points (**Fig. 6b**). Several approximate models have been reported for the relationship between flash points and boiling points (Costa do Nascimento et al., 2020; Santos et al., 2020). In addition, oxidation stability is an important property that characterizes fuel quality for long-term

Please cite this article as: Liu J., Molina E.R., Moiser N.S. Sustainable biokerosene from lipids using efficient ozone cracking. Biofuel Research Journal 46 (2025) 2412-2431. DOI: 10.18331/BRJ2025.12.2.4.

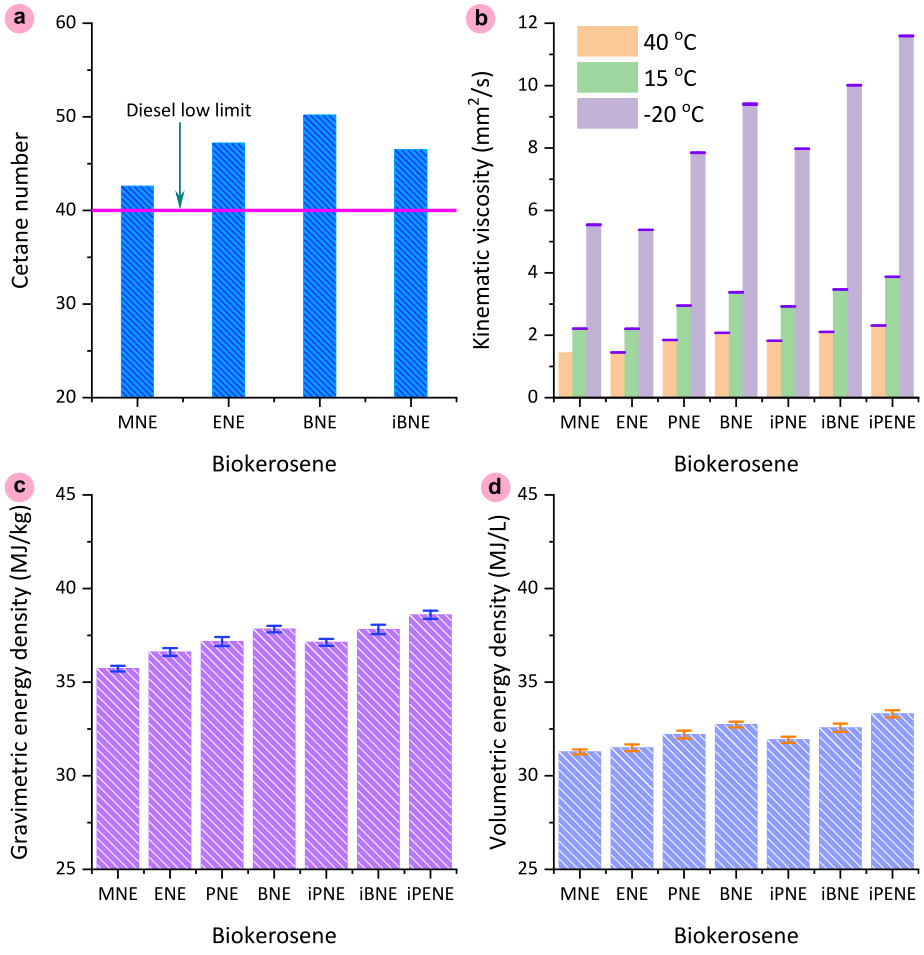

Fig. 5. (a) Cetane numbers of biokerosene; **(b)** kinematic viscosity of biokerosene at various temperatures; **(c)** gravimetric energy density of biokerosene; and **(d)** volumetric energy density of biokerosene.

atmospheric storage. Biokerosene did not show oxidation even after 100 h of oxidation stability tests using the EN 15751 method (**Table 3**). Since soybean oil is highly enriched with unsaturated compounds (> 85%), the oxidation stability of soy biodiesel is generally short (e.g., <2 h) and less than the specification for biodiesel. This phenomenon indicates that antioxidants are required to improve the oxidation stability to meet the specification, which will increase the biodiesel production cost. Compared to biodiesel, compounds in biokerosene are fully saturated structures, which results in excellent oxidation stability (e.g., > 100 h). Super long oxidation stability can allow biokerosene to be stored in the atmosphere without degradation and reduce the production costs caused by the antioxidant's consumption.

The diesel distillation temperature curve operated under reduced pressure indicates the composition of light and heavy components. A small T50 (distillation temperature of 50% of fuel) indicates a high fraction of light components, while a large T90 (distillation temperature of 90% of fuel) shows a low fraction of light components. Biodiesel has a limitation of T90 less than 360 ºC, and jet fuel has a limitation of T90 less than 300 ºC. In addition, jet fuel has a limitation of T10 (distillation temperature of 10% of fuel) above 205 ºC. The boiling points detected at 1 atm are less than jet fuel's T90 limitation and greater than jet fuel's T10 limitation, which shows biokerosene can be potentially used as jet fuel or blended with jet fuel. TGA analysis also indicated the boiling points of biokerosene (**Fig. 6c**). The onset temperatures of boiling and the end temperatures of boiling obtained from TGA were less than the measured normal boiling points because of the increased evaporation rates by nitrogen gas (**Figs. S33-S42**).

The monoglycerides and sterol glucosides precipitate above the cloud point for the biodiesel from current feedstocks. However, the biokerosene showed no issue with the cold soak filtration test because the feedstock is the FFA instead of triglycerides. The cold soak filtration test for the typical biokerosene showed excellent performance (**Fig. 7**). The cold soak filtration test slightly increased with the carbon chain length of the alcohols. In addition, the isomerized alcohol used in synthesis also resulted in slightly increased values of the cold soak filtration test. The cold soak filtration test for biokerosene was much less than the measured soy biodiesel (120 seconds) and the biodiesel limit (360 seconds).

3.3. Gas emission analysis of biokerosene and biokerosene/jet fuel blends

Carbon chain length, C/H ratio, carbon-carbon double bond, and O/C ratio significantly influence diesel/biodiesel emissions (McCormick and Colorado, 1998; Jafarihaghighi et al., 2020; Liu et al., 2023b). Biokerosene is saturated FAEs with middle carbon chain lengths, while current biodiesel consists of long carbon chain fatty acid methyl esters (FAMEs) with carbon chain lengths of 16 and 18. Compared to hydrocarbon diesel, oxygen atoms in biodiesel and synthesized biokerosene facilitate combustion in the engine, resulting in decreased UHC (**Fig. 8a**) and CO emissions (**Fig. 8b**) and increased CO_2 emissions (**Fig. 8c**). However, the effect of oxygen on emission is not linearly related to oxygen percentage in the molecules.

Please cite this article as: Liu J., Molina E.R., Moiser N.S. Sustainable biokerosene from lipids using efficient ozone cracking. Biofuel Research Journal 46 (2025) 2412-2431. DOI: 10.18331/BRJ2025.12.2.4.

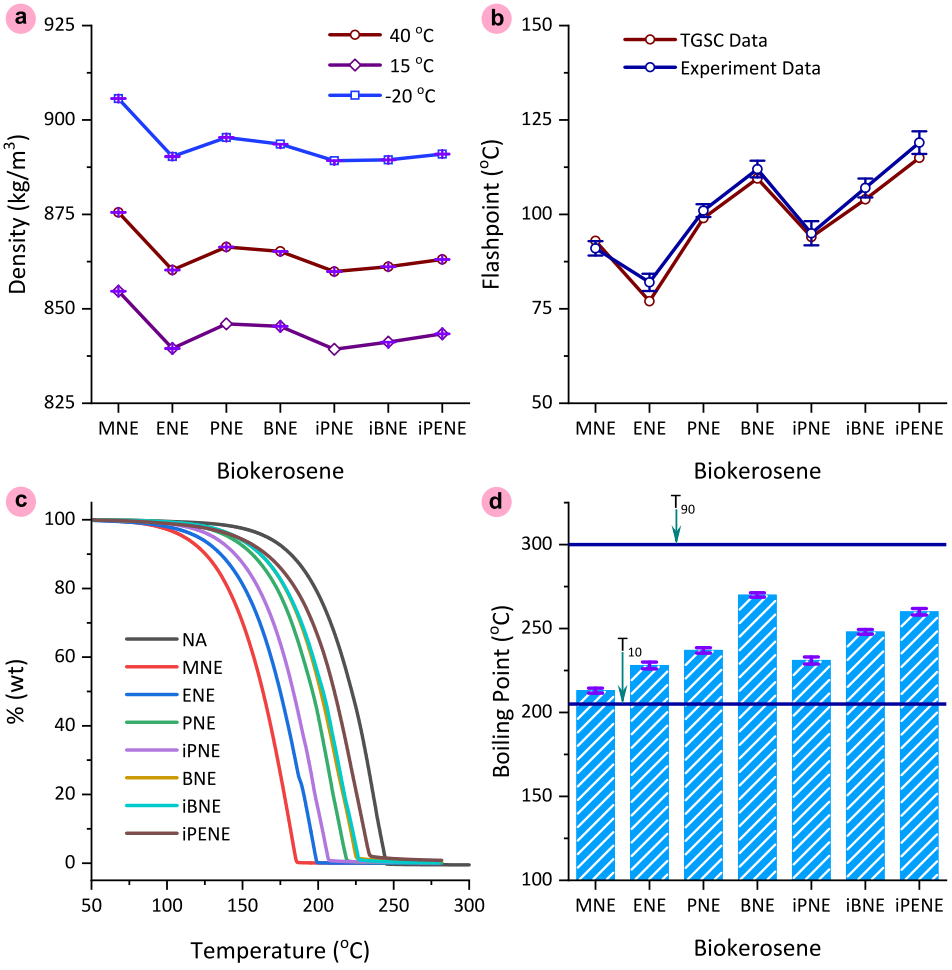

Fig. 6. **(a)** Densities at various temperatures; **(b)** Flashpoints; **(c)** TGA analysis of nonanoic acid and esters; and **(d)** Measured boiling points.

Table 3.
Oxidation stability of biokerosene and soy biodiesel using EN 15751.

Fuel		Oxidation Stability (Hours)
Specification for biodiesel		> 3
Specification for biodiesel/diesel blend		> 6
Biokerosene	MNE	>100
	ENE	
	PNE	
	BNE	
	iPNE	
	iBNE	
	iPENE	
Soy biodiesel		<2

Synthesized biokerosene, with shorter carbon-chain lengths than biodiesel, contains a higher percentage of oxygen, yet it produces higher UHC and CO emissions compared to biodiesel. When different alcohols are used in synthesis, the resulting biokerosene shows reduced oxygen content with increasing alcohol molecular weight; however, there is no clear relationship between oxygen content and complete combustion.

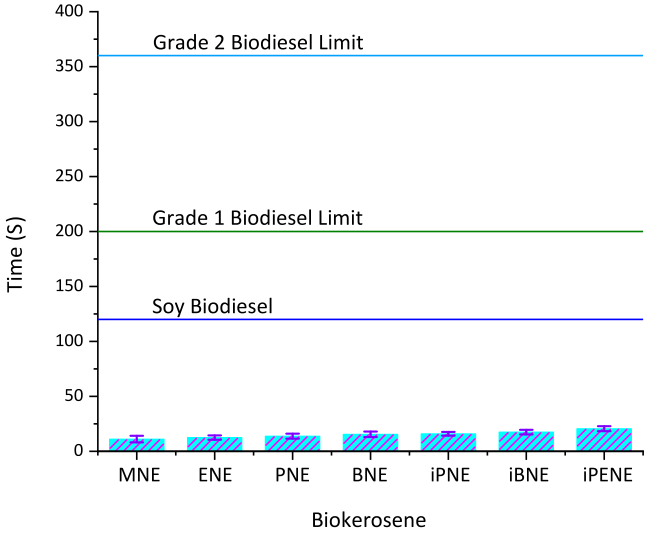

Fig. 7. Cold soak filtration test of biokerosene according to ASTM D 7501.

Please cite this article as: Liu J., Molina E.R., Moiser N.S. Sustainable biokerosene from lipids using efficient ozone cracking. Biofuel Research Journal 46 (2025) 2412-2431. DOI: 10.18331/BRJ2025.12.2.4.

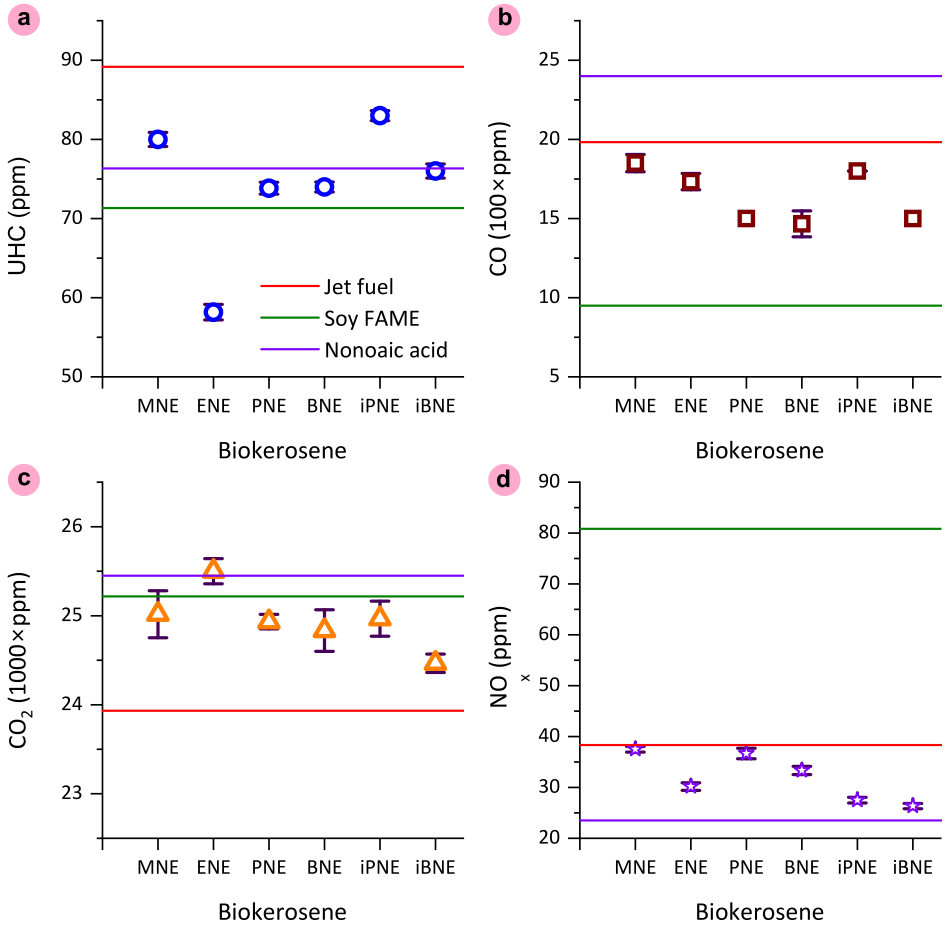

Fig. 8. Emission analysis of synthesized biokerosene in a diesel engine, **(a)** unburned hydrocarbon (UHC); **(b)** carbon monoxide (CO); **(c)** carbon dioxide (CO_2); and **(d)** nitrogen oxides (NO_x) emissions.

These observations suggest that other properties, such as droplet size during combustion, also influence combustion efficiency. The primary factor affecting droplet size is viscosity: biokerosene generally has lower viscosity than biodiesel, leading to larger droplets. Therefore, both oxygen content and physical properties (e.g., viscosity) act in concert to influence combustion behavior in diesel engines, as further evidenced by the performance of biokerosene-jet fuel blends.

Cloud points, kinematic viscosities, and flash points of ENE/jet fuel blends were measured (Fig. 9). Cloud points decreased with the increased jet fuel fractions (Fig. 9a) while kinematic viscosities increased with the jet fuel fractions. Flashpoint dramatically decreased for jet fuel fractions below 50% and did not significantly change above 50% (Fig. 9c). The emissions of ENE/jet fuel blends were measured after combustion in the diesel engine. With the increased jet fuel in the blends, the emission of CO_2 decreased (Fig. 10c), and the emissions of UHC (Fig. 10a) and CO (Fig. 10b) increased. In addition, blending a small amount of biokerosene (e.g., 25 vol%) with jet fuel can significantly improve combustion. Soot or particulate matter (PM) formation is strongly influenced by the degree of unsaturation and can be characterized by the hydrogen-to-carbon (H/C) ratio.

Due to being fully saturated, biokerosene is expected to result in much less PM emissions than biodiesel with a significant level of unsaturated FAMEs. NO_x are GHG emissions typically produced during high-temperature combustion and have approximately 300 times the global warming potential (GWP) of CO_2. Carbon-carbon double bonds in the molecules can significantly affect NO_x emissions. Soy FAMEs can result in about two times NO_x emissions as jet fuel (Fig. 8d). Synthesized biokerosene is saturated and can result in much less NO_x emissions and slightly less than jet fuel. The biokerosene (ENE) blending with jet fuel also shows that NO_x emissions decreased with increased biokerosene fractions (Fig. 10d). In addition to carbon-carbon double bonds, the carbon chain length also affects NO_x emissions. The longer the carbon chain length, the higher the combustion temperature. High combustion temperature will result in higher NO_x emissions. Jet fuel has a slightly longer average carbon chain length than nonanoic acid, resulting in slightly higher NO_x emissions (Fig. 8d). Moreover, to differentiate the effect of oxygen-related functional groups on combustion, we compare the combustion behaviors of nonanoic acid with biodiesel, nonanoates, and jet fuel. Both carboxylic and ester functional groups can increase the emissions of CO_2 and reduce the emissions of UHCs and NO_x, especially for NO_x reduction. However, carboxylic groups can cause increased CO emissions (Fig. 8b).

3.4. Current and future biokerosene synthesis

Biokerosene production depends on two feedstocks: unsaturated lipids (e.g., oleic acid) and alcohol. Oleic acid can be broadly obtained from oil and fats, especially high oleic oil. High oleic oil is a new oil variety, and the projected high oleic soybean oil production in the United States is about 4 million tons in 2024 (Hassan, 2023) and will reach over 20 million tons in the next several years. However, oils serve as a major source for food and feedstock for biofuel and bioproducts. To overcome the production limitation, lipid production through sugar fermentation has also been developed (Dowe, 2019). The most abundant sugar resource is biomass,

Please cite this article as: Liu J., Molina E.R., Moiser N.S. Sustainable biokerosene from lipids using efficient ozone cracking. Biofuel Research Journal 46 (2025) 2412-2431. DOI: 10.18331/BRJ2025.12.2.4.

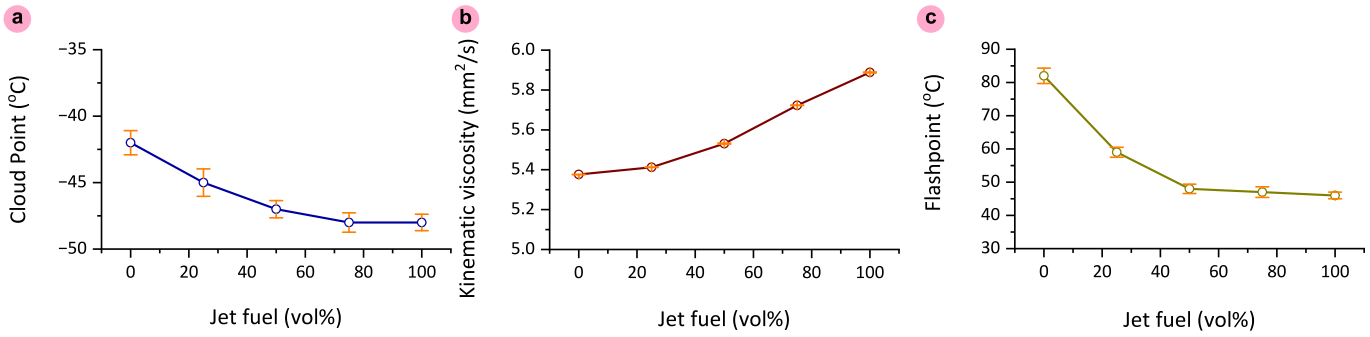

Fig. 9. Primary properties of ENE/Jet fuel blends: **(a)** cloud points; **(b)** kinematic viscosity; and **(c)** flashpoints.

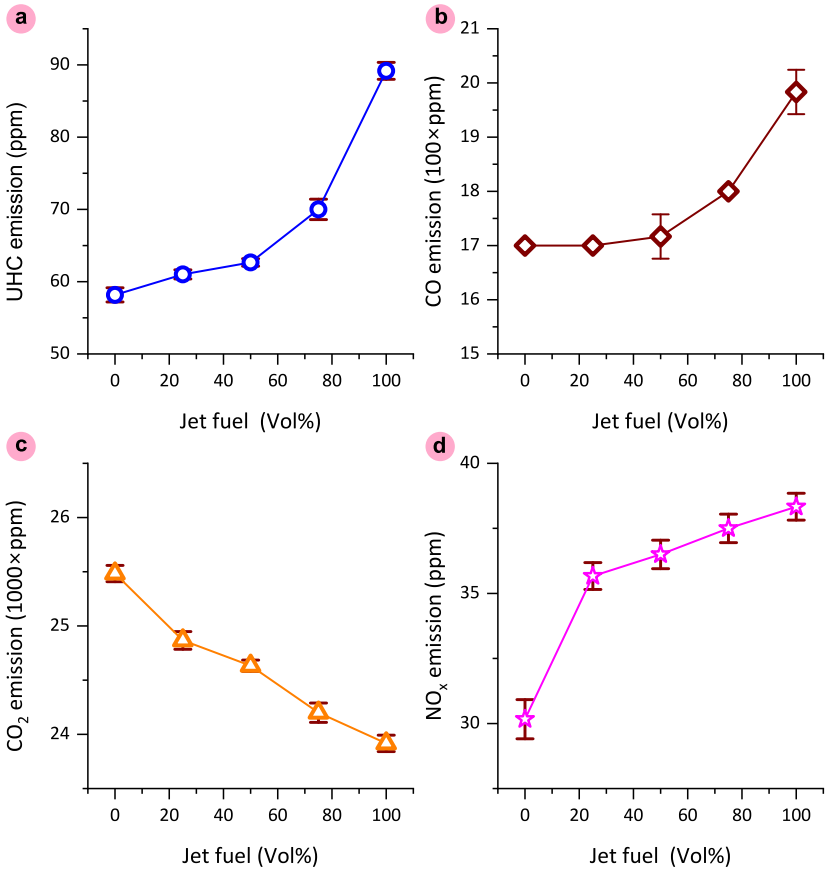

Fig. 10. Emission analysis of biokerosene-jet fuel blenders: **(a)** unburned hydrocarbon (UHC); **(b)** carbon monoxide (CO); **(c)** carbon dioxide (CO_2); and **(d)** nitrogen oxides (NO_x) emissions.

which can be obtained from agricultural residue, forestry waste, and algae. The current biomass production in the United States is about 342 million tons per year, and it potentially can reach over 1 billion tons per year in the future (Seay, 2024). A typical biomass contains about 30~55% of cellulose, 15~60% of hemicellulose, and 10~30% of lignin, depending on the sources (Williams et al., 2017; Liu and Beckerman, 2022). The average fermentable materials (cellulose and hemicellulose) in biomass account for about 75%. The theoretical lipid yield through fermentation is 0.3 g lipids/g sugar, and a study has shown lipid yield from sugar fermentation can reach about 0.27 g lipids/g sugar (Matthew et al., 2022). Oleic acid in high oleic oil accounts for at least 75% and up to 90%, and the average oleic acid content in high oleic oil is 80%. Therefore, the annual production rate of oleic acid in the United States from high oleic soybean oil will be about 3.2 million metric tons (MMT) in 2024 and can reach 16 MMT in the future. Lipids from biomass-derived sugar fermentation in the United States could be about 69 MMT and reach over 200 MMT in the future. Oleic acid content in the fermented lipids can be at least 50%. Consequently, oleic acid from fermented lipids can be around 35 MMT and reach over 100 MMT in the

Please cite this article as: Liu J., Molina E.R., Moiser N.S. Sustainable biokerosene from lipids using efficient ozone cracking. Biofuel Research Journal 46 (2025) 2412-2431. DOI: 10.18331/BRJ2025.12.2.4.

future. In summary, the total available oleic acid in the United States can be around 40 MMT now and reach over 116 MMT in the future.

The other main feedstock in biokerosene production is alcohol. Though many alcohols can be used for synthesizing esters with nonanoic acid from ozone cracking of oleic acid, the availability of the alcohols, the qualities of biokerosene, and production cost should be considered together. The typical alcohol used in current biodiesel production is methanol for its low price, large availability, and low production cost. However, methanol is mainly produced from the chemical synthesis of petroleum-based materials. Therefore, the renewability of biokerosene from methanol is impaired. Another largely available alcohol is ethanol, mainly commercially produced *via* fermentation, with an annual production rate of over 16 BGal in the United States (Liu et al., 2023a). With the electrification of passenger cars, this technology presented in this study will provide a new use for bioethanol instead of its current use as an additive to gasoline. In addition, n-butanol and isobutanol can also be produced from the fermentation process. These fermentation processes for bio-alcohol production are characterized by low alcohol concentrations in the fermentation broth, typically 1–14% for bioethanol and around 1% for butanol. Since distillation is the conventional method for alcohol recovery, energy consumption increases significantly as the feed concentration decreases. Moreover, conventional distillation cannot produce pure alcohol due to the presence of azeotropes in the aqueous solution. Other technologies are also developed to reduce GHG emissions in the refining process, such as fully electrified ultrasonic separation (Liu et al., 2023a and 2025; Liu and Feng, 2024). Another method to obtain bio-alcohols is via pyrolysis of woody biomass under high temperatures and pressures. However, multiple alcohols are produced in this process, and ethanol is the main product (Bain et al., 2014). Alcohol can also be converted from syngas ($CO+H_2$) by the Fischer-Tropsch process, but this energy consumption and capital investment are much higher. Therefore, ENE is preferred at the current stage according to its properties, ethanol availability, and renewability.

According to the mass balance of oleic acid to biokerosene (**Fig. 11**), one metric ton of oleic acid can be converted to about 202.8 gallons of ENE by consuming 162.8 kg of ethanol, or 231.5 gallons of BNE by consuming 262.3 kg of butanol. Considering the most available alcohol being ethanol, the potential ENE biokerosene annual production rate is predicted based on current and future oleic acid availability (**Fig. 12**). ENE biokerosene production can reach approximately 0.65 BGal using high oleic soybean oil, requiring about 0.17 BGal of ethanol. Alternatively, production can reach around 7.10 BGal using fermented lipids, consuming approximately 1.9 BGal of ethanol. Therefore, this technology can provide nearly 8 BGal of biokerosene to the United States to replace fossil-based diesel or jet fuel. In the future, this technology can provide about 23.5 BGal of ENE biokerosene to the United States. Meanwhile, about 18 BGal of ethanol will be consumed in the production, which means the bioethanol produced in the United States can be fully used.

In addition to the route shown in this study, a process is developed to synthesize RD or SAF using alcohol through dehydration, oligomerization, and hydrogenation. Compared to this route, utilization of alcohol in biokerosene production is a better choice because of the following reasons: 1) no need for the expensive catalyst and the maintenance cost, 2) atmospheric pressure and low reaction temperature, 3) uniform products without the fractionation process, 4) no need for the high carbon footprint hydrogen sources, 5) low mass fractions loss utilization of alcohol. Weight losses from dehydration of ethanol and butanol are 40% and 25%, respectively. With the commercialized technology of ozone cracking and esterification process, the provided technology can easily adopt the current biodiesel process, compared to current technologies with low technology readiness levels.

3.5. Challenges and perspectives on scale-up and commercialization

In addition to developing a production process on new sites, biokerosene production can be constructed in the lipid (crops or fermented lipids) extraction facilities or biodiesel facilities. The co-location of biodiesel production is preferred because: 1) it is flexible to upgrade biodiesel to biokerosene according to the weather limits or market demand; 2) it is easily adapted to the safety and other regulations with respect to fuel production and storage; and 3) it may take advantage of the existing infrastructures, such as storage, logistics, etc. In term of co-location with biodiesel production, both ozone cracking of lipids and ozone cracking of biodiesel can be used (**Fig. 13**). Compared to biodiesel production, the major difference is the ozone cracking process in biokerosene synthesis. Ozone cracking has been used in wastewater treatment on a commercial scale, and the technology can be used in biodiesel upgrading. Here, the ozone level after reaction should be recycled until it meets the EPA regulations.

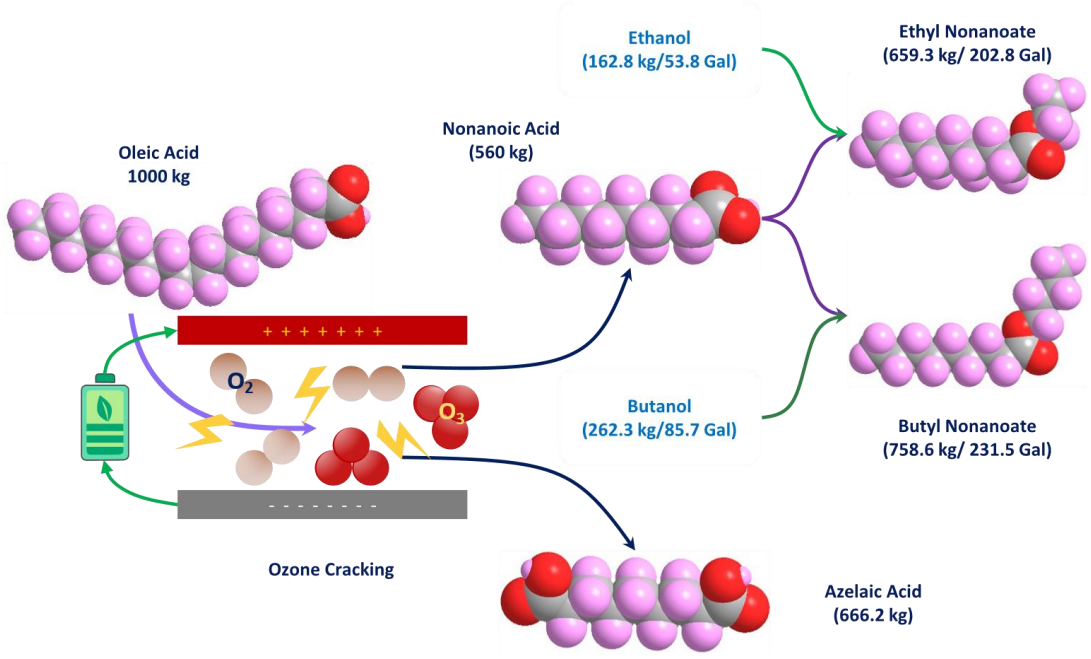

Fig. 11. Schematic process of biokerosene production from oleic acid.

Please cite this article as: Liu J., Molina E.R., Moiser N.S. Sustainable biokerosene from lipids using efficient ozone cracking. Biofuel Research Journal 46 (2025) 2412-2431. DOI: 10.18331/BRJ2025.12.2.4.

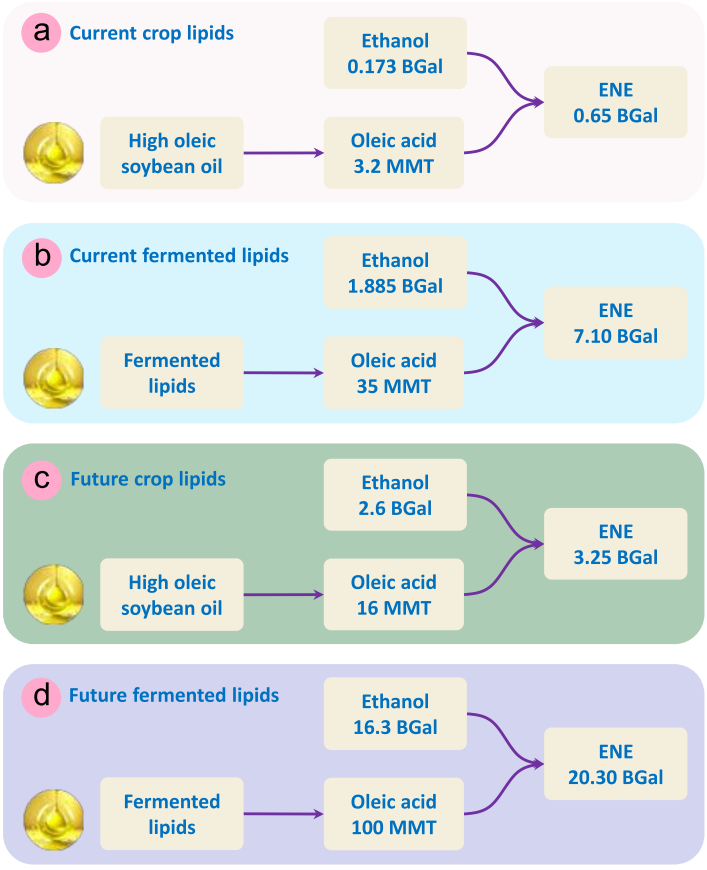

Fig. 12. Predicted annual ENE biokerosene production rate in the United States from various sources. **(a)** current high oleic soybean oil annual production rate; **(b)** lipids obtained from biomass through fermentation at the current biomass annual production rate; **(c)** future high oleic soybean oil annual production rate; and **(d)** lipids obtained from biomass through fermentation at the future biomass annual production rate.

The critical properties of biokerosene were compared with the specifications of diesel, jet fuel, biodiesel, and biodiesel/diesel blends (Table 4). Compared to biodiesel, biokerosene has many advantages, and the most essential qualities of biokerosene are the ultra-low cloud point and super-long oxidation stability. The ultra-low cloud point shows biokerosene can be used in cold environments, such as winter-season diesel and jet fuel. The super-long oxidation stability shows that biokerosene is suitable for long-term storage without adding antioxidants to preserve biokerosene qualities. Biokerosene can be used as an alternative to diesel and biodiesel. Compared to diesel, biokerosene takes advantage of low aromatic levels, which indicate the potential to reduce soot and NO_x emissions. Based on the cloud point range, biokerosene can replace NO.1 diesel. Biokerosene can be either purely used or blended with #2 diesel for cold environments, depending on the specific temperature requirements. Biokerosene can meet or exceed the specifications for jet fuel.

However, there are some challenging specifications for biokerosene utilization as jet fuel. Some types of biokerosene (e.g., BNE, iBNE, and iPENE) have high viscosities (> 8 mm^2/s), which indicates they must be blended with jet fuel to reduce the viscosity. Current specifications for jet fuel are developed based on hydrocarbon fuels, which require that jet fuel has a low FAME percentage (< 0.5%) when using lipids as feedstocks. However, this study provides a new synthesis route using middle-chain FAE as jet fuel, and this specification is unsuitable for biokerosene. Additionally, compared to hydrocarbon-based diesel and jet fuel, biokerosene has about 10 to 15% less energy density due to the presence of the ester function group.

3.6. Preliminary techno-economic analysis (TEA) and life cycle assessment (LCA)

Preliminary TEA and LCA were performed to estimate the economic aspect and sustainability of biokerosene production using ozone-cracked high-oleic soybean oil. In addition, preliminary TEA and LCA were also performed for fatty acid ethyl ester (FAEE) as biodiesel production using high-oleic soybean oil with ethanol as an alcohol, and RD/SAF production from high-oleic soybean oil. The biokerosene can be separated into two types: ENE as No. 1 biokerosene (No.1 BK) with a cloud point below -40 ^oC and diethyl azelate ester (DEAE) as No. 2 biokerosene (No.2 BK) with a cloud point of about -20 ^oC. The parameters of input, output, energy consumption, prices, and carbon intensity used for preliminary TEA and LCA are shown in Tables 5 to 8.

The mass-based yields based on input high oleic soybean oil follow in the order: RD/SAF < No.1 BK < No.2 BK < FAEE < biokerosene (Fig. 14a). FAEE yield can be over one due to the molecular weight of ethanol being greater than 1/3 of the molecular weight of the glycol functional group. Total biokerosene can reach about 1.3 because 1) the molecular weight of ozone-cracked oil is greater than that of unreacted oil, and 2) ethanol is used in transesterification and esterification in biokerosene synthesis. According to the costs of fuel production in Equation 2, high oleic soybean oil contributes a significant portion to the total cost of fuel production (Fig. 14b). Without considering the co-products' values, the costs of fuel production follow as No.1 BK > RD/SAF > No.2 BK > BK > FAEE. However, the costs of fuel production can be significantly reduced by considering the co-products' values, especially for biokerosene production (Fig. 14c). The fluctuation of material prices also affects the

Please cite this article as: Liu J., Molina E.R., Moiser N.S. Sustainable biokerosene from lipids using efficient ozone cracking. Biofuel Research Journal 46 (2025) 2412-2431. DOI: 10.18331/BRJ2025.12.2.4.

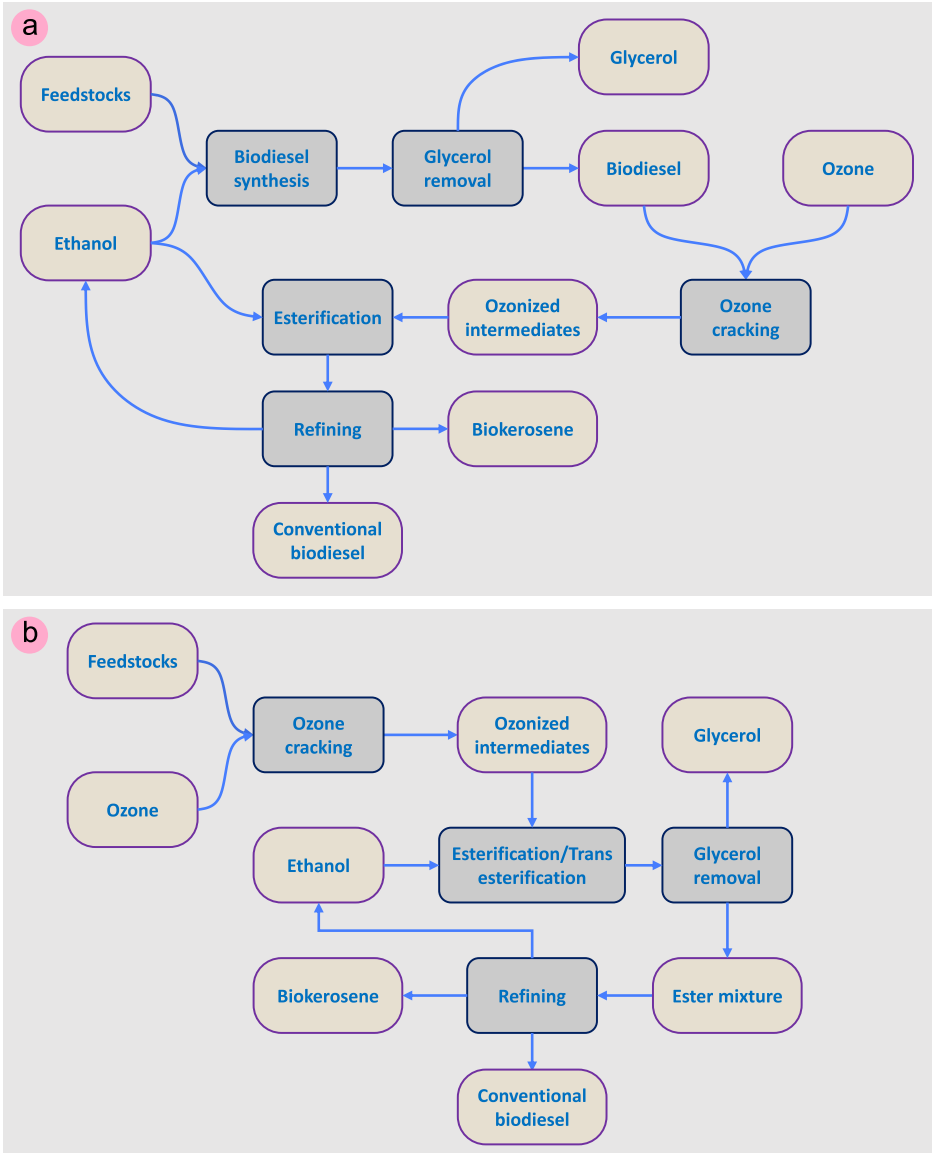

Fig. 13. Scheme of biokerosene co-location with biodiesel production facility. **(a)** upgrading biodiesel to biokerosene after biodiesel synthesis, **(b)** ozone cracking of lipids before biodiesel synthesis.

costs of biokerosene with a baseline of USD 0.978/kg biokerosene, especially for high oleic soybean oil (Fig. 14d).

$$\mathrm{Cost_{fuel}} = \sum(\mathrm{AMT}_i \times \mathrm{Price}_i)\,/\mathrm{AMT_{fuel}} \qquad \text{Eq. 2}$$

Where, $\mathrm{Cost_{fuel}}$ is the cost of fuel production (USD/kg fuel); $\mathrm{AMT_i}$ is the amount of materials or energy used to produce fuel (Table 5); $\mathrm{Price_i}$ is the unit price for materials or energy (Table 6); and $\mathrm{AMT_{fuel}}$ is the amount of fuel produced.

The energy usage and carbon intensities of materials were used to estimate the CO_2-eq emissions according to Equation 3 (Fig. 15). The CO_2-eq emissions follow the order RS/SAF > biokerosene > FAEE biodiesel. When considered separately, No. 1 biokerosene (ENE) and No. 2 biokerosene (DEAE) show high CO_2-eq emissions, since they are two major products with a ratio of about 2 to 3 in the fuel production. CO_2-eq emissions can be significantly reduced when they are combined in the evaluation (Fig. 15a). In biokerosene production, CO_2-eq emissions from various sectors follow ethanol > oil > ozone > utility.

$$\mathrm{CI_{fuel}} = \sum(\mathrm{AMT}_i \times CI_i)\,/EC_{\mathrm{fuel}} \qquad \text{Eq. 3}$$

where, $\mathrm{CI_{fuel}}$ is the CO_2-eq emission of fuel (g CO/MJ); $\mathrm{AMT_i}$ is the amount of materials or energy used to produce fuel (Table 5); $\mathrm{CI_i}$ is the unit carbon intensity of materials or energy (Tables 7 and 8); and $\mathrm{EC_{fuel}}$ is the energy content of fuel produced.

Current ethanol production uses corn as the major feedstock, which has relatively high carbon intensity because of the high energy required for refining using distillation (Liu et al., 2023a; Liu and Feng, 2024). With the electrification of refining using the ultrasonic process, the potential of the CO_2-eq emissions in refining can be reduced by over 90% using carbon-neutral electricity (Ha et al., 2024). With the feedstock shifting from food-based corn to non-food-based lignocellulose, the carbon intensity of bioethanol can be further reduced and potentially reach zero. When carbon-neutral bioethanol is used, the carbon intensity of biokerosene is reduced

Please cite this article as: Liu J., Molina E.R., Moiser N.S. Sustainable biokerosene from lipids using efficient ozone cracking. Biofuel Research Journal 46 (2025) 2412-2431. DOI: 10.18331/BRJ2025.12.2.4.

Table 4.
Evaluation of biokerosene according to the critical specifications of diesel, jet fuel, and biodiesel [A].

Property Specifications	ASTM test method	Diesel		Jet Fuel	Biodiesel	Biodiesel/ Diesel	Biokerosene[B]
		No.1	No.2				
Standard		D975		D 7566	D 6751		
Flash point, °C,	D 93	>38	>52	>38	>93	>93	75-120
Kinematic viscosity, mm^2/s @ 40 °C	D 445	1.3-2.4	1.9-4.1	–	1.9-6.0	–	1.4-1.9
Kinematic viscosity, mm^2/s @ -20 °C	D 445	–	–	<8.0	–	–	5.5-12
Cetane Number	D976	>40	>40	–	>45	>40	43-52
Oxidation stability, hours	EN15751	–	–	–	>3	>6	>100
Aromaticity, vol%	D1319	35	35	0.5	–	35	–
Distillation temperature, 90%, °C	D86	<288	282-338		<360	<343	–
Distillation temperature, 10%, °C	D86	–	–	<205	–	–	–
Final boiling point, °C	D86	–	–	<300	–	–	210-280
Density, kg/m^3	D56	820-845	820-845	775-840	860-900	–	860-870
Cloud point, °C	D2500	Up to -28	<-40	–			-35 – -67
Freezing point, °C	D 5972	–	–	<-40	–	–	-35 – -67
Cold soak filtration test, seconds	D 7501	–	–	–	200/360		<25
FAME, mg/kg	IP585	–	–	<5	–	–	
Volumetric energy density, MJ/L[C]		36	36	>33 [D]	33	–	31-33
Gravimetric energy density, MJ/kg[C]		43	43	>42.8[D]	38	–	36-38

A: The limits for each specification are obtained from the ASTM standards (ASTM D 975, 2022; ASTM D 6751, 2023; ASTM D 7566, 2022).
B: Value range based on various alcohol
C: Typical values
D: Specific requirements for jet fuel

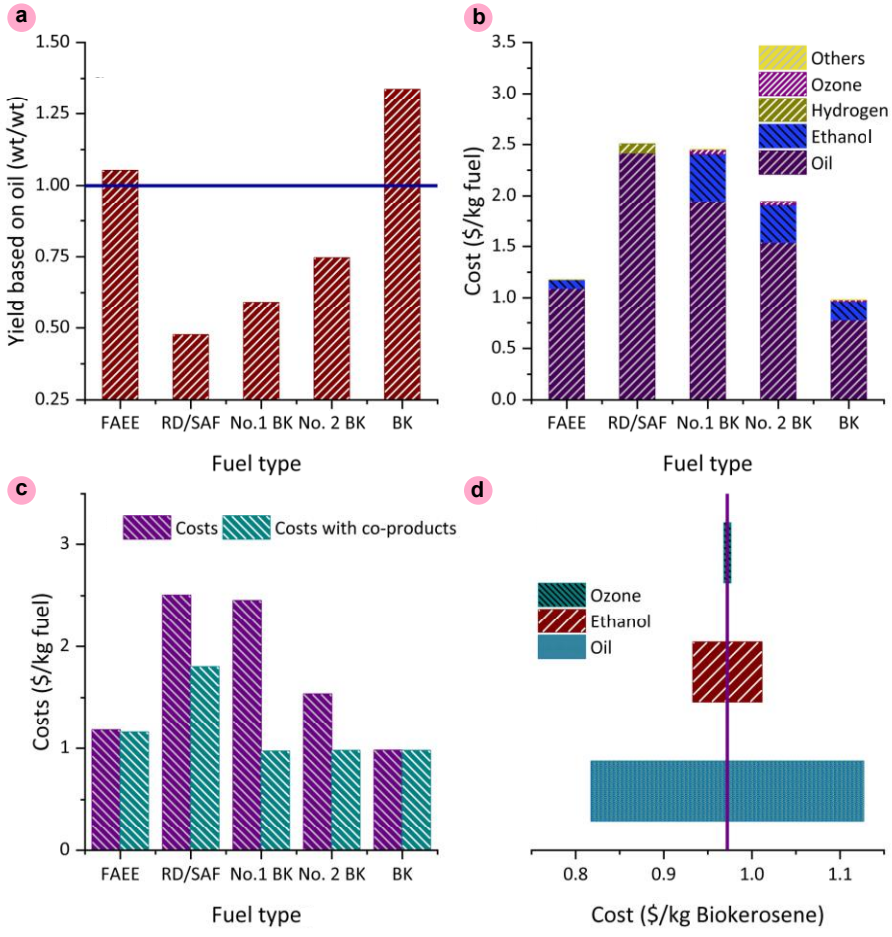

Fig. 14. Preliminary TEA analysis of FAEE, RD/SAF, and biokerosene: **(a)** mass yield of fuel with respect to the high oleic soybean oil input; **(b)** breakdown costs of fuel production; **(c)** comparison of fuel costs with/without considering co-products; and **(d)** effect of price fluctuations (± 20%) on the biokerosene (ENE+DEAE) cost (FAEE: Fatty acid ethyl ester; BK: Biokerosene).

Please cite this article as: Liu J., Molina E.R., Moiser N.S. Sustainable biokerosene from lipids using efficient ozone cracking. Biofuel Research Journal 46 (2025) 2412-2431. DOI: 10.18331/BRJ2025.12.2.4.

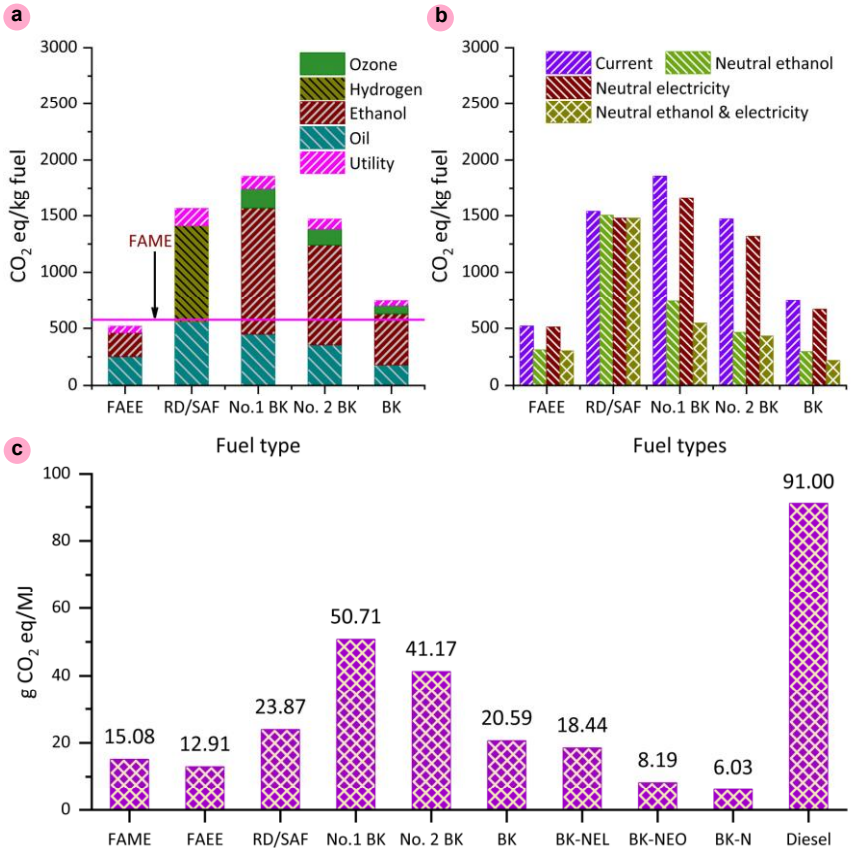

Fig. 15. Preliminary LCA analysis of fuel production from high oleic soybean oil: **(a)** breakdown of CO_2-eq emission from various sectors; **(b)** CO_2-eq emission of fuel under current operation, future carbon-neutral electricity, future carbon-neutral ethanol; and **(c)** CO_2-eq emission based on fuel energy under various conditions (BK-NEO is biokerosene production using carbon-neutral ethanol; BK-NEL is biokerosene production using carbon-neutral electricity; and BK-N is biokerosene production using both carbon-neutral ethanol and carbon-neutral electricity).

Table 5.
Inventory of 1 kg biodiesel, RD/SAF, and biokerosene from high oleic soybean oil*.

	Biodiesel	RD/SAF	Biokerosene
Feedstock input (kg/kg fuel)	0.95	2.1	1.69
Energy input (MJ/kg fuel)			
Heating	1.0	1.83	1.9
Electric	0.1	0.7	0.2
Materials input (g/kg fuel)			
Hydrogen	–	75	–
Ethanol	150	–	805
Sodium hydroxide	4	–	
Sulfuric acid	–	–	4
Ozone	–	–	280
Outputs (kg/kg fuel)			
Biodiesel/FAEE	1	–	0.18
RD/SAF	–	1	–
Naphtha	–	0.56	–
No.1 Biokerosene ENE (T_{cp}<-40°C)	–	–	1
No.2 Biokerosene DEAE (T_{cp}<-20°C)	–	–	1.26
LPG	–	0.33	–
Glycerol	0.1	–	0.19

* Operation parameters using the previously published data for biodiesel (Xu et al., 2022) and SAF (Xu et al., 2020).

Table 6.
Manufacturing costs.

	Unit	Value	Ref.
Raw materials			
High oleic soybean oil *	USD/ton	1150	
Hydrogen	USD/ton	1200	Dagdougui et al. (2018)
Ethanol	USD/ton	570	USDA AMS (2025)
Ozone **	USD/ton	160	
Sodium hydroxide	USD/ton	310	businessanalytiq.com (2025a)
Sulfuric acid	USD/ton	115	businessanalytiq.com (2025b)
Utilities			
Electric power	USD/kWh	0.08	U.S. EIA (2025a)
Natural gas (LHV=38.42)	USD/m^3	0.20	U.S. EIA (2025b)
Product prices			
LPG	USD/ton	1200	U.S. EIA (2025c)
Naphtha	USD/ton	550	Trading Economics (2025)
Glycerol	USD/ton	220	Xu et al. (2022)

* High oleic soybean oil is estimated based on soybean oil with slightly increased.
** Ozone cost is calculated based on the electricity used for ozone generation and the electricity cost.

from 799.1 g CO_2-eq/kg biokerosene to 295.0 g CO_2-eq/kg biokerosene (Fig. 15b). Ozone production significantly contributes to CO_2-eq emissions, accounting for approximately 10% of the total emissions in biokerosene production.

Please cite this article as: Liu J., Molina E.R., Moiser N.S. Sustainable biokerosene from lipids using efficient ozone cracking. Biofuel Research Journal 46 (2025) 2412-2431. DOI: 10.18331/BRJ2025.12.2.4.

Table 7.
Energy consumption for chemical production.

Material	Unit	Value	Ref.
Hydrogen	MJ/kg	44.5	IEA (2023)
Ozone	kWh/kg	2	Jodzis and Zięba (2018)

Table 8.
Carbon intensity of chemicals and energy.

Material	Unit	Value	Ref.
High oleic soybean oil	g CO_2/kg	265	Nagapurkar and Smith (2023)
Ethanol	g CO_2/kg	1390	Scully et al. (2021)
Hydrogen	g CO_2/kg	11400	IEA (2023)
Ozone *	g CO_2/kg	630	
Electric power	g CO_2/kWh	315	U.S. EIA (2024b)
Natural gas	g CO_2/MJ	50	U.S. EIA (2024a)

* Ozone carbon intensity is calculated based on the electricity used for ozone generation and the electricity carbon intensity.

As the carbon intensity of electricity continues to decline and approaches carbon neutrality, the carbon intensity of biokerosene can be further reduced to 217.5 g CO_2-eq/kg biokerosene (**Fig. 15b**). Carbon emissions based on the energy generated from each fuel were compared (**Fig. 15c**). At the current stage, GHG emission reduction follows the trend: FAEE biodiesel (85.7%) > FAME biodiesel (83.4%) > biokerosene (77.3%) > RD/SAF (77.3%). When both carbon-neutral electricity and carbon-neutral ethanol are used, the carbon emissions associated with biokerosene production can be reduced by more than 93%.

4. Conclusions

This study presents a novel process for synthesizing biokerosene from nonanoic acid, the primary product from the ozone cracking of high oleic oil, with various alcohols. The type of alcohol used in the synthesis significantly influenced the properties of biokerosene from this process. Generally, biokerosene synthesized in this study exhibits excellent oxidation stability because of the saturation of the molecules. The excellent oxidation stability indicates that the resulting fuel can be stored stably without the addition of antioxidants. In addition, the biokerosene synthesized in this study also expressed excellent low-temperature performance. Biokerosene from this process can be used as winter season diesel, kerosene, or jet fuel because the cloud points range from -35 to -67 ^oC. Biokerosene from this process has flash points ranging from 75 to 120 ^oC, which indicates that it is safer than diesel for handling and storage. Biokerosene in this study had no issue with cold soak filtration as it has no relation to monoglycerides and sterol glucosides. Biokerosene in this research expressed sufficient or better cetane numbers. Biokerosene in this research showed a minimum energy density above 35 MJ/kg. Based on the current availability of alcohol, sustainability, and production cost, ENE is the best choice at the current stage. With energy-efficient separation technology development, such as membrane separation and ultrasonic process intensification, BNE or iBNE may become the predominant biokerosene for the winter season or jet fuel. Preliminary TEA shows that the production cost can be about USD 0.978/kg biokerosene when considering the co-products' value. Preliminary LCA shows the carbon intensity of biokerosene is about 779 g CO_2-eq/kg biokerosene or 20.6 g CO_2-eq/MJ. Compared to fossil hydrocarbon fuels, biokerosene can reduce emissions by over 77% at current operation and can further reduce emissions by over 93% when using carbon-neutral ethanol and electricity in the near future. In summary, biokerosene provided in this research provided a novel economic and sustainable route to produce jet fuel or winter season diesel fuel.

Acknowledgments

We appreciated the financial support for this research from the Indiana Soybean Alliance, grant numbers ISA VC3-SFY23-026, VC3-SFY24-124, and VC3-SFY24-175. We acknowledge the help from all faculty, staff, and students in the LORRE lab in this project. We acknowledged Dr. Gozdem Kilaz for assisting with analyzing viscosity, density, and energy contents. The Research Instrumentation Center at Purdue University is gratefully acknowledged for providing FTIR and MS analysis. Iowa Central Fuel Testing Laboratory and Southwest Research Institute were gratefully acknowledged for providing the tests for oxidation stability and cetane number, respectively.

References

[1] ASTM D 7566, 2022. Standard specification for aviation turbine fuel containing synthesized hydrocarbons. ASTM International.
[2] ASTM D 975, 2022. Standard specification for aviation turbine fuel containing synthesized hydrocarbons. ASTM International.
[3] ASTM D 6751, 2023. Standard specification for biodiesel fuel blend stock (B100) for middle distillate Fuels. ASTM International.
[4] Bain, R.L., Magrini-Bair, K.A., Hensley, J.E., Jablonski, W.S., Smith, K.M., Gaston, K.R., Yung, M.M., 2014. Pilot scale production of mixed alcohols from wood. Ind. Eng. Chem. Res. 53(6), 2204-2218.
[5] Baliban, R.C., Elia, J.A., Floudas, C.A., Xiao, X., Zhang, Z., Li, J., Cao, H., Ma, J., Qiao, Y., Hu, X., 2013. Thermochemical conversion of duckweed biomass to gasoline, diesel, and jet fuel: process synthesis and global optimization. Ind. Eng. Chem. Res. 52(33), 11436-11450.
[6] businessanalytiq.com, 2025a. Sodium hydroxide price index.
[7] businessanalytiq.com, 2025b. Sulfuric acid price index.
[8] Chong, C.T., Ng, J.H., 2021.Vhapter- Biojet fuel production pathways, in: biojet fuel in aviation applications. Elsevier, pp. 81-141.
[9] Costa do Nascimento, D., Dorighello Carareto, N.D., Marinho Barbosa Neto, A., Gerbaud, V., da Costa, M.C., 2020. Flash point prediction with UNIFAC type models of ethylic biodiesel and binary/ternary mixtures of FAEEs. Fuel. 281, 118717.
[10] Dagdougui, H., Sacile, R., Bersani, C., Ouammi, A., 2018. Chapter2-hydrogen production and current technologies, in: Hydrogen infrastructure for energy applications. Elsevier, pp. 7-21.
[11] Davis, R., Tao, L., Scarlata, C., E.C.D., T., Ross, J., Lukas, J., Sexton, D., 2015. Process design and economics for the conversion of lignocellulosic biomass to hydrocarbons: dilute-acid and enzymatic deconstruction of biomass to sugars and catalytic conversion of sugars to hydrocarbons, National Renewable Energy Laboratory.
[12] De Jong, S., Antonissen, K., Hoefnagels, R., Lonza, L., Wang, M., Faaij, A., Junginger, M., 2017. Life-cycle analysis of greenhouse gas emissions from renewable jet fuel production. Biotechnol. Biofuels. 10(1), 64.
[13] De Jong, S., Hoefnagels, R., Faaij, A., Slade, R., Mawhood, R., Junginger, M., 2014. The feasibility of short-term production strategies for renewable jet fuels-a comprehensive techno-economic comparison. Biofuels Bioprod. Biorefin. 8(6), 743.
[14] Diederichs, G.W., Ali Mandegari, M., Farzad, S., Görgens, J.F., 2016. Techno-economic comparison of biojet fuel production from lignocellulose, vegetable oil and sugar cane juice. Bioresour. Technol. 216, 331-339.
[15] Dowe, N., 2019. DOE Bioenergy Technologies Office (BETO) 2019 Project Peer Review.
[16] Fakayode, O.A., Akpabli-Tsigbe, N.D.K., Wahia, H., Tu, S., Ren, M., Zhou, C., Ma, H., 2021. Integrated bioprocess for bio-ethanol production from watermelon rind biomass: ultrasound-assisted deep eutectic solvent pretreatment, enzymatic hydrolysis and fermentation. Renewable Energy. 180, 258-270.
[17] Ha, J.W., Liu, J., Feng, H., Sahinidis, N. V., Seo, H., Siirola, J.J., Na, J., 2024. Ultrasound-based separation of ethanol-water mixtures is economically advantageous and sustainable. Cell. Rep. Phys. Sci. 5(2), 101785.
[18] Han, J., Tao, L., Wang, M., 2017. Well-to-wake analysis of ethanol-to-jet and sugar-to-jet pathways. Biotechnol. Biofuels. Bioprod. 10(1).
[19] Hassan, Z., 2023. An overview of the development of high oleic soybean oil in the United States and its implication on palm oil.
[20] IEA, 2021. Global hydrogen review 2021, OECD Publishing.
[21] IEA, 2023. Comparison of the emissions intensity of different hydrogen production routes.

Please cite this article as: Liu J., Molina E.R., Moiser N.S. Sustainable biokerosene from lipids using efficient ozone cracking. Biofuel Research Journal 46 (2025) 2412-2431. DOI: 10.18331/BRJ2025.12.2.4.

[22] Jafarihaghighi, F., Ardjmand, M., Salar Hassani, M., Mirzajanzadeh, M., Bahrami, H., 2020. Effect of fatty acid profiles and molecular structures of nine new source of biodiesel on combustion and emission. ACS Omega. 5(26), 16053-16063.
[23] Jodzis, S., Zięba, M., 2018. Energy efficiency of an ozone generation process in oxygen. Analysis of a pulsed DBD system. Vacuum. 155, 29-37.
[24] Kourkoumpas, D., Sagani, A., Hull, A., Hull, A., Karellas, S., Grammelis, P., 2024. Life cycle assessment of an innovative alcohol-to-jet process: the case for retrofitting a bioethanol plant for sustainable aviation fuel production. Renewable Energy. 228.
[25] Kruger, J.S., Cleveland, N.S., Yeap, R.Y., Dong, T., Ramirez, K.J., Nagle, N.J., Lowell, A.C., Beckham, G.T., McMillan, J.D., Biddy, M.J., 2018. Recovery of fuel-precursor lipids from oleaginous yeast. ACS Sustainable Chem. Eng. 6(3), 2921-2931.
[26] Liu, J., Beckerman, J., 2022. Application of sustainable biosorbents from hemp for remediation of copper(II)-containing wastewater. J. Environ. Chem. Eng. 10(3), 107494.
[27] Liu, J., Feng, H., 2024. Experimental and theoretical analysis of ultrasonic separation in bioethanol purification. Results in Eng. 24, 102886.
[28] Liu, J., Pearlstein, A.J., Feng, H., 2025. Effects of operating parameters on single-stage ultrasonic separation of ethanol from its aqueous solutions. Sep. Purif. Technol. 353(Part A), 128179.
[29] Liu, J., Tao, B., 2022a. Thermodynamically predicting liquid/solid phase change of long-chain fatty acid methyl esters (FAMEs) and its application in evaluating the low-temperature performance of biodiesel. J. Taiwan. Inst. Chem. Eng. 135, 104384.
[30] Liu, J., Tao, B., 2022b. Fractionation of fatty acid methyl esters *via* urea inclusion and its application to improve the low-temperature performance of biodiesel. Biofuel Res. J. 9(2), 1617-1629.
[31] Liu, J., Pearstein, A.J., Feng, H., 2023a. Ultrasonic separation in bioethanol refining. Chem. Eng. Prog. 119(3), 24-30.
[32] Liu, J., Tao, B.Y., Feng, H., Mosier, N.S., 2023b. Efficient rapid fractionation of fatty acid methyl esters (FAMEs) through evaporative urea inclusion. Chem. Eng. J. 454(Part 3), 140266.
[33] Liu, J., Zhang, C., Tao, B., Beckerman, J., 2023c. Revealing the roles of biomass components in the biosorption of heavy metals in wastewater by various chemically treated hemp stalks. J. Taiwan. Inst. Chem. Eng. 143, 104701.
[34] Mailaram, S., Maity, S.K., 2022. Dual liquid–liquid extraction *versus* distillation for the production of bio-butanol from corn, sugarcane, and lignocellulose biomass: a techno-economic analysis using pinch technology. Fuel. 312, 122932.
[35] Malins, K., 2021. Synthesis of renewable hydrocarbons from vegetable oil feedstock by hydrotreatment over selective sulfur-free SiO_2-Al_2O_3 supported monometallic Pd, Pt, Ru, Ni, Mo and bimetallic NiMo catalysts. Fuel. 285, 119129.
[36] Matlock, M.G., 2022. Introduction: the need for high-oleic oils, High Oleic Oils. Elsevier Inc.
[37] Matthew, W., Ryan, D., Jake, K., 2022. Algal biomass conversion to fuels via combined algae processing (CAP): 2021 state of technology and future research. Golden, CO. National Renewable Energy Laboratory. NREL/TP-5100-82502.
[38] McCormick, M.S.G. and R.L., Colorado, 1998. Combustion of fat and vegetable oil derived fuels in diesel engines. Prog. Energy Combust. Sci. 24(97), 125-164.
[39] Nagapurkar, P., Smith, J.D., 2023. Techno-economic and life cycle analyses for a supercritical biodiesel production process from waste cooking oil for a plant located in the Midwest United States. Environ. Dev. Sustainable. 1-25.
[40] Naidu, H., Liu, J., Kahraman, O., Feng, H., 2021. Ultrasound-assisted nonthermal, nonequilibrium separation of organic molecules from their binary aqueous solutions: effect of solute properties on separation. ACS Sustainable Chem. Eng. 9(48), 16506-16518.
[41] Nogales-Delgado, S., Encinar, J.M., González Cortés, Á., 2021. High oleic safflower oil as a feedstock for stable biodiesel and biolubricant production. Ind. Crops. Prod. 170, 113701.
[42] Nowatzki, J., Shrestha, D., Swenson, A., Wiesenborn, D., 2019. Biodiesel cloud point and cold weather issues.
[43] Orjuela, A., Paulo, C., Cadavid, J.G., García-nunez, J.A., 2022. Experimental optimization during epoxidation of a high-oleic palm oil using a simplex algorithm. Ind. Crops Prod. 187(Part A), 115321.
[44] Ou, Y., West, J.J., Smith, S.J., Nolte, C.G., Loughlin, D.H., 2020. Air pollution control strategies directly limiting national health damages in the US. Nat. Commun. 11(1), 957.
[45] Santos, S.M., Nascimento, D.C., Costa, M.C., Neto, A.M.B., Fregolente, L. V., 2020. Flash point prediction: reviewing empirical models for hydrocarbons, petroleum fraction, biodiesel, and blends. Fuel. 263, 116375.
[46] Scully, M.J., Norris, G.A., Alarcon Falconi, T.M., MacIntosh, D.L., 2021. Carbon intensity of corn ethanol in the United States: state of the science. Environ. Res. Lett. 16.
[47] Seay, S., 2024. Sustainable biomass production capacity could triple US bioeconomy.
[48] Shin, J., Kim, D., Seo, J., Park, S., 2020. Effects of the physical properties of fuel on spray characteristics from a gas turbine nozzle. Energy. 205, 118090.
[49] Smith, C.J., Forster, P.M., Allen, M., Fuglestvedt, J., Millar, R.J., Rogelj, J., Zickfeld, K., 2019. Current fossil fuel infrastructure does not yet commit us to 1.5 °C warming. Nat Commun 10(1), 101.
[50] Tat, M.E., Van Gerpen, J.H., 1999. The kinematic viscosity of biodiesel and its blends with diesel fuel. JAOCS, J. Am. Oil Chem. Soc. 76(12), 1511-1513.
[51] TGSC, The good scents company information system.
[52] Trading Economics, 2025. Naphtha.
[53] U.S. EIA, 2023. Monthly energy review, monthly energy review.
[54] U.S. EIA, 2024a. Carbon dioxide emission coefficients.
[55] U.S. EIA, 2024b. How much carbon dioxide is produced per kilowatthour of U.S. electricity generation?
[56] U.S. EIA, 2025a. Electric power monthly.
[57] U.S. EIA, 2025b. Indiana natural gas industrial price.
[58] U.S. EIA, 2025c. Weekly Indiana propane residential price.
[59] USDA AMS, 2025. National weekly ethanol report.
[60] Voeten, R.L.C., Hendriks, F., Bezemer, G.L., 2024. Fischer-tropsch synthesis for the production of sustainable aviation fuel: formation of tertiary amines from ammonia contaminants. ACS Omega. 9 (29), 31974-31985.
[61] Walkling, C.J., Doppalapudi, K.R., Zhang, D.D., Harvey, B.G., 2025. Renewable diesel fuel prepared by the isomerization and hydrogenation of biosynthetic farnesene. Energy Fuels. 39(18), 8495-8500.
[62] Wang, W.-C., Tao, L., Markham, J., Zhang, Y., Tan, E., Batan, L., Biddy, M., Wang, W.-C., Tao, L., Zhang, Y., Tan, E., Warner, E., Biddy, M., 2016. Review of biojet fuel conversion technologies. Golden, CO. National Renewable Energy Lab. NREL/TP-5100-66291.
[63] Wei, H., Liu, W., Chen, X., Yang, Q., Li, J., Chen, H., 2019. Renewable bio-jet fuel production for aviation: a review. Fuel. 254, 115599.
[64] Williams, L., Emerson, R., Tumulura, J.S., 2017. Biomass compositional analysis for conversion to renewable fuels and chemicals, in: Biomass volume estimation and valorization for energy. InTech.
[65] Xu, H., Lee, U., Wang, M., 2020. Life-cycle energy use and greenhouse gas emissions of palm fatty acid distillate derived renewable diesel. Renew. Sust. Energy Rev. 134, 110144.
[66] Xu, H., Ou, L., Li, Y., Hawkins, T.R., Wang, M., 2022. Life cycle greenhouse gas emissions of biodiesel and renewable diesel production in the United States. Environ. Sci. Technol. 56(12), 7512-7521.
[67] Xue, C., Cheng, C., 2019. Chapter Two-Butanol production by *Clostridium*. 1st ed, Advances in bioenergy. Elsevier Inc.
[68] Zoppi, G., Tito, E., Bianco, I., Pipitone, G., Pirone, R., Bensaid, S., 2023. Life cycle assessment of the biofuel production from lignocellulosic biomass in a hydrothermal liquefaction-aqueous phase reforming integrated biorefinery. Renewable Energy. 206, 375-385.

Please cite this article as: Liu J., Molina E.R., Moiser N.S. Sustainable biokerosene from lipids using efficient ozone cracking. Biofuel Research Journal 46 (2025) 2412-2431. DOI: 10.18331/BRJ2025.12.2.4.

Dr. Junli Liu is a principal investigator and senior research scientist in the Department of Agricultural and Biological Engineering and Laboratory of Renewable Resources Engineering at Purdue University. In addition to research, he also teaches courses on modeling and thermodynamics. He received his PhD at Purdue University in 2012 and worked in the biofuel industry after graduation, with roles in quality control, process development, and research. He worked as a research scientist at Purdue University from 2016 to 2018 on using hemp to make biosorbents for wastewater treatment and synthesizing cellulose nanocrystals. He became an academic researcher at the University of Illinois at Urbana-Champaign in 2019 and worked to develop ultrasonic separation from laboratory batch scale to continuous pre-pilot plant scale. He has been awarded as PI or Co-PI by various funding agencies. His research interests lie in renewable energy, biofuels and bioproducts, biorefining, separation, process intensification, carbon sequestration, and nanoparticles. His research profile on Google Scholar can be found at the following link: https://scholar.google.com/citations?hl=es&user=L2lYrZYAAAAJ

Dr. Elena A. Robles Molina holds a Ph.D. in Agricultural and Biological Engineering from Purdue University in West Lafayette, IN. Working at LORRE, her research centered on the synthesis and characterization of high-performance lubricants and polyols from soybean oils. She is currently an R&D chemist at Ivanhoe Industries in Zion, IL. Her research interests include organic synthesis of nonionic surfactants and lubricants, enzyme-catalyzed reactions, and advanced analytical chemistry techniques. She is committed to developing sustainable, bio-based alternatives to petrochemical products. Her research profile on Google Scholar can be found at the following link: https://scholar.google.com/citations?hl=es&user=McLsi1IAAAAJ

Dr. Nathan S. Mosier is the Indiana Soybean Alliance New Uses Professor and Head of Agricultural and Biological Engineering at Purdue University. His research focuses on bioprocess engineering for transforming carbohydrates (starch and cellulose) and lipids (vegetable oils) found in agricultural products into energy, fuels, polymers, and chemicals. He develops novel catalysts, reaction engineering, reactor design, and process integration from his research. His research profile on Google Scholar can be found at the following link: https://scholar.google.com/citations?user=gTKen7kAAAAJ&hl=en

Please cite this article as: Liu J., Molina E.R., Moiser N.S. Sustainable biokerosene from lipids using efficient ozone cracking. Biofuel Research Journal 46 (2025) 2412-2431. DOI: 10.18331/BRJ2025.12.2.4.

Supplementary Material

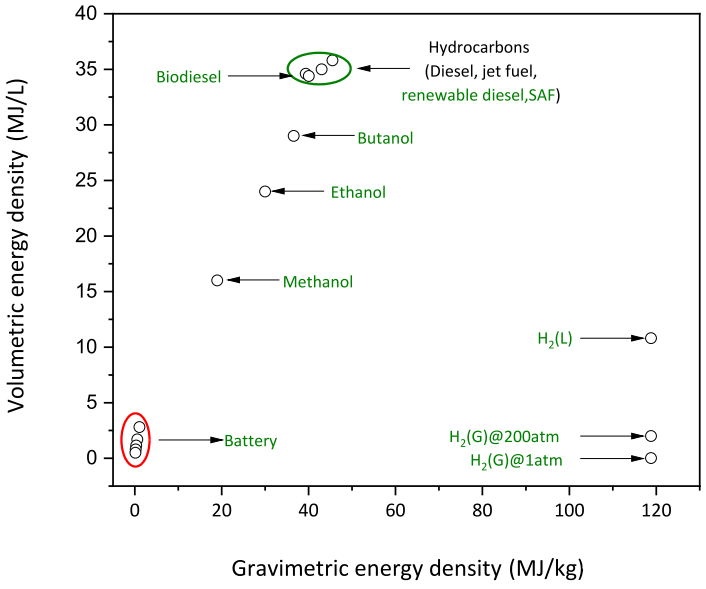

Fig. S1. Comparison of energy density for various renewable energy sources. Hydrogen shows the best gravimetric energy density of about 119 MJ/kg, but volumetric energy density depends on the states, with the maximum volumetric energy density being about 10.8 MJ/L (Kurz et al., 2022). Hydrocarbons show the best volumetric energy density (46 MJ/kg), and biodiesel is about 15 % less (Liu et al., 2023). Alcohol energy densities increase with carbon chain length (Xue and Cheng, 2019; Liu et al., 2022). At the current stage, battery technology indicates worse energy density (Weimar, 2020).

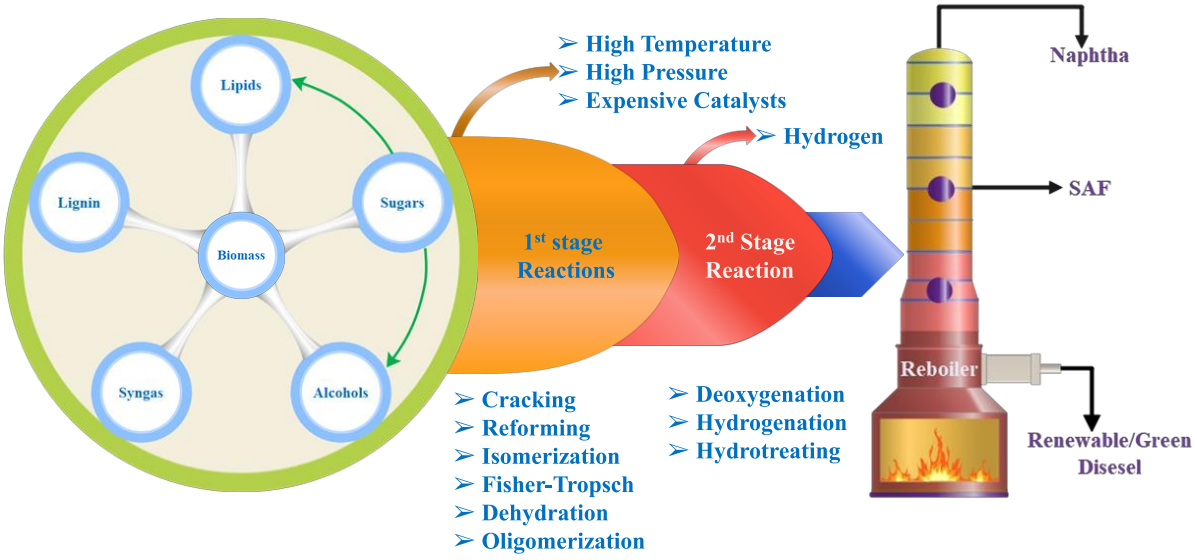

Fig. S2. Summary of routes to hydrocarbons. Fats/oils, biomass-derived syngas, biomass-derived sugars, and biomass-derived alcohols are the main feedstocks for synthesizing hydrocarbons through catalytic hydrotreating at high pressure and high temperature. The products need to be fractionated into naphtha, sustainable aviation fuel (SAF), and renewable diesel fuel for the widespread carbon chain length and isomers.

Please cite this article as: Liu J., Molina E.R., Moiser N.S. Sustainable biokerosene from lipids using efficient ozone cracking. Biofuel Research Journal 46 (2025) 2412-2431. DOI: 10.18331/BRJ2025.12.2.4.

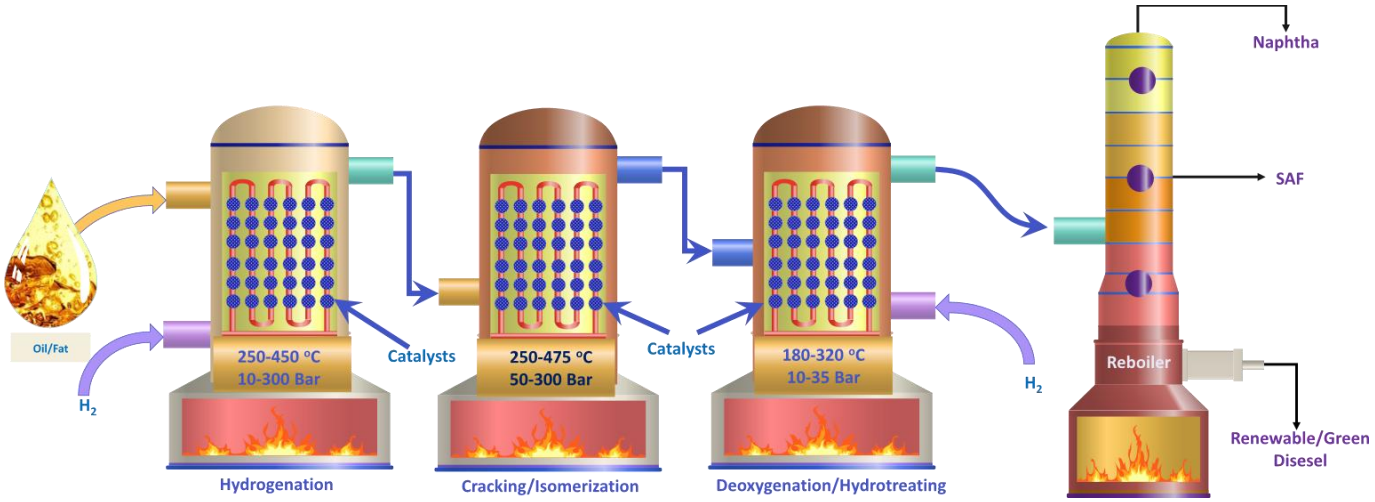

Fig. S3. Synthesis of hydrocarbons from fats, oils, and free fatty acids (FFA). Direct hydrogenation of fats/oils/FFA can produce hydrocarbons, but the products own poor low-temperature performance due to the long carbon chain length. Fats/oils/FFAs need to be thermally or catalytically cracked into small molecules or isomerized to improve the low-temperature performance. In addition, deoxygenation and hydrotreating are necessary to reduce the contents of oxygen, alkene, and aromatics.

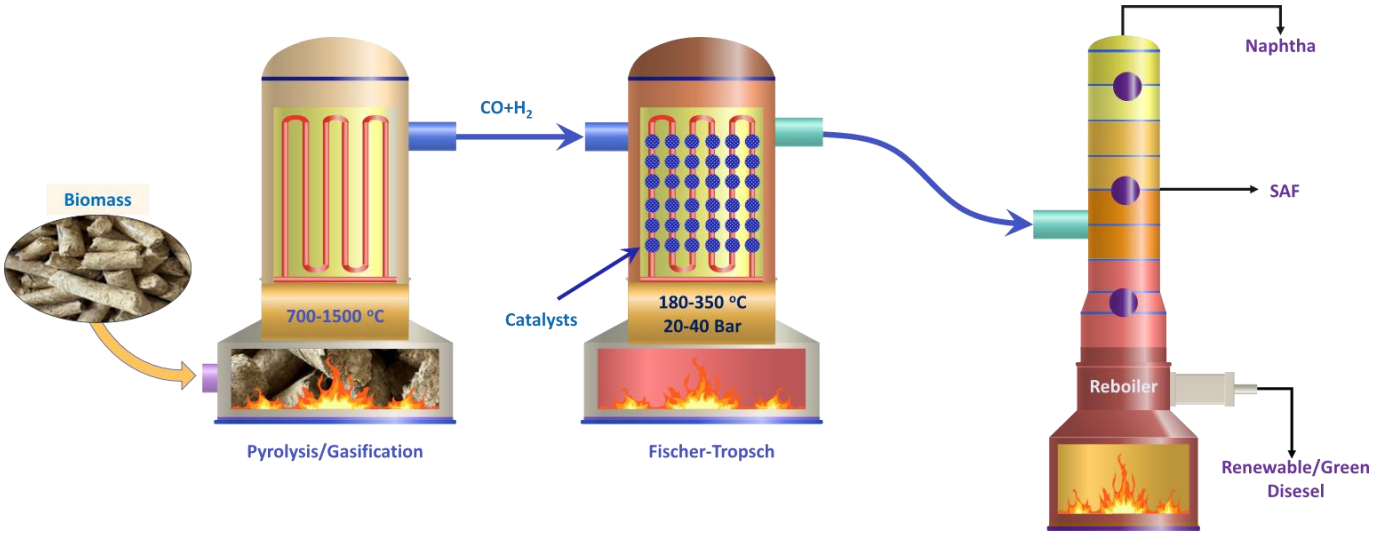

Fig. S4. Synthesis of hydrocarbons from syngas. Biogas is converted from biomass by pyrolysis or gasification. Then, syngas works as the feedstock to synthesize the hydrocarbons by the Fischer-Tropsch process with catalysts and hydrogen. The resulting hydrocarbons go through distillation to obtain various categories of production, such as naphtha, SAF, and renewable diesel.

Please cite this article as: Liu J., Molina E.R., Moiser N.S. Sustainable biokerosene from lipids using efficient ozone cracking. Biofuel Research Journal 46 (2025) 2412-2431. DOI: 10.18331/BRJ2025.12.2.4.

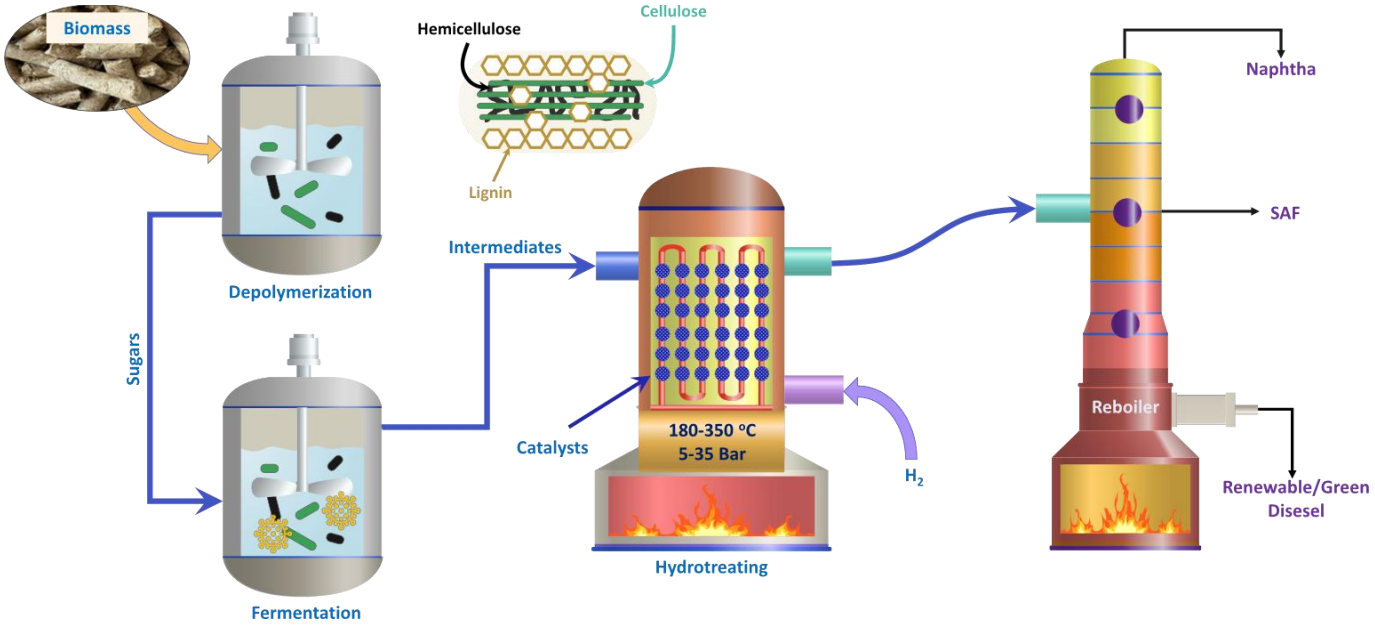

Fig. S5. Direct sugar to hydrocarbons.

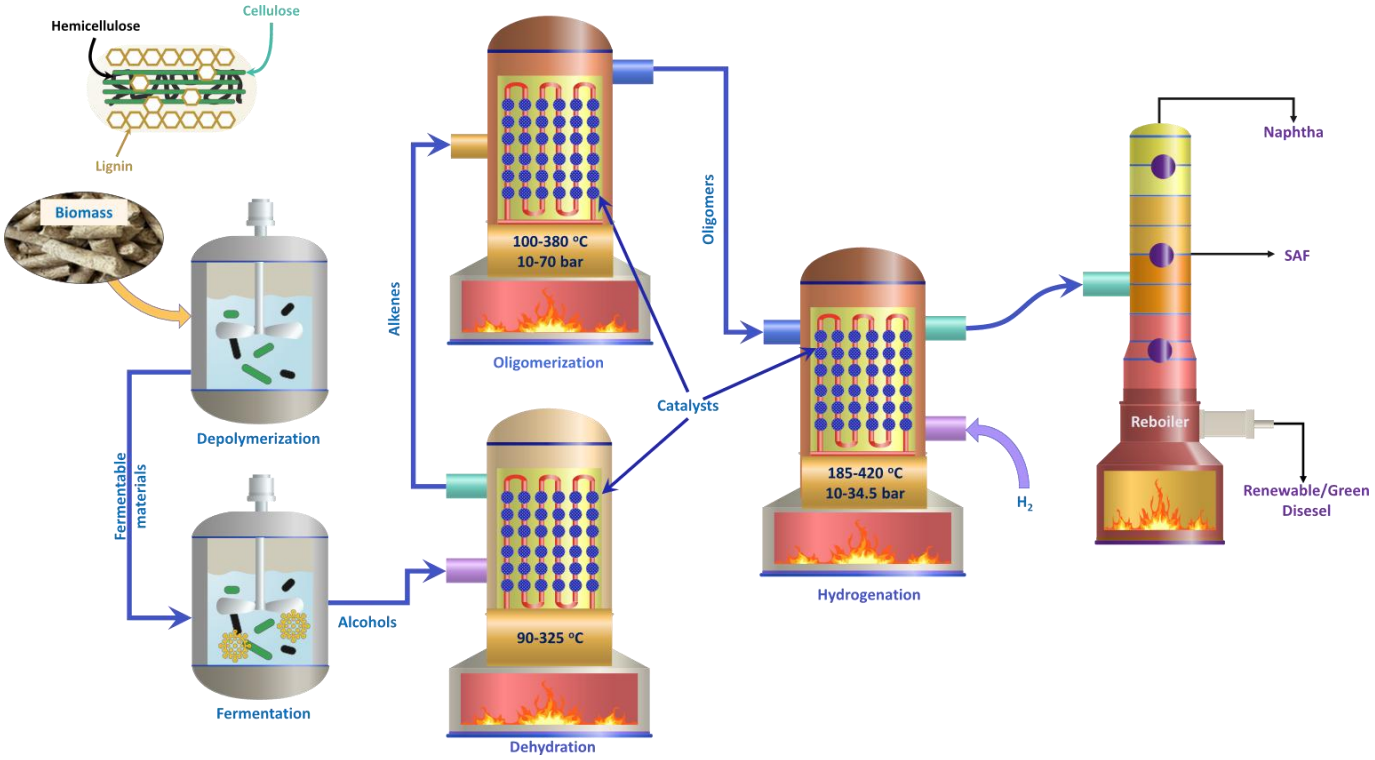

Fig. S6. Synthesis of hydrocarbons from biomass-based alcohol.

Please cite this article as: Liu J., Molina E.R., Moiser N.S. Sustainable biokerosene from lipids using efficient ozone cracking. Biofuel Research Journal 46 (2025) 2412-2431. DOI: 10.18331/BRJ2025.12.2.4.

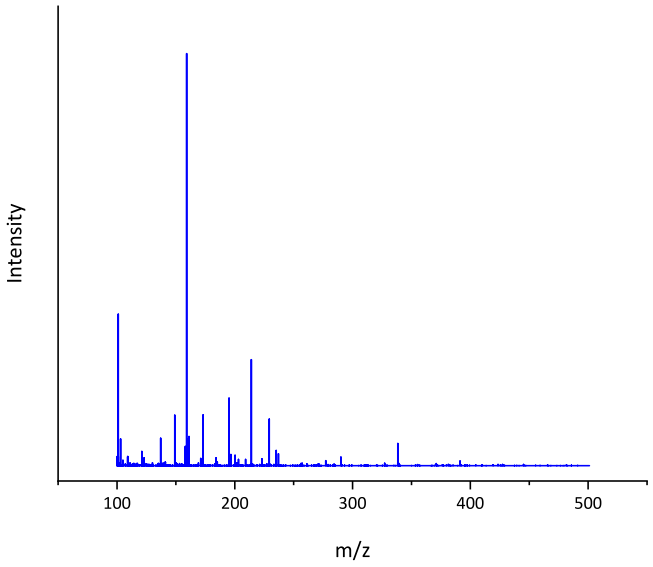

Fig. S7. Mass spectra of nonanoic acid.

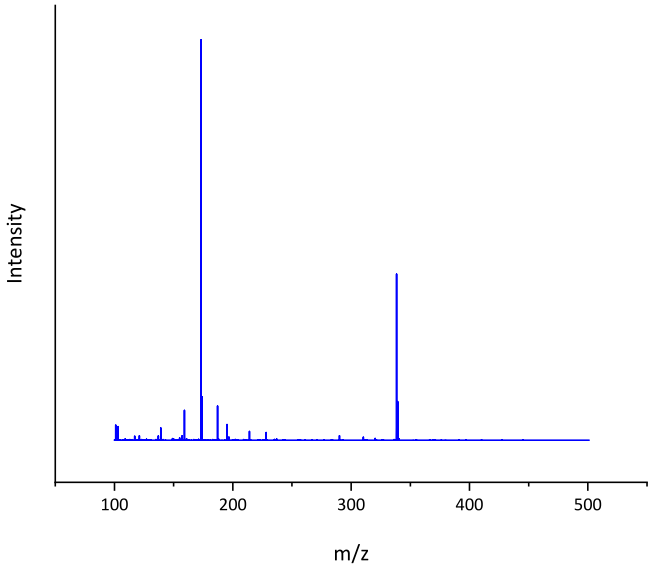

Fig. S8. Mass Spectra of methyl nonanoate (MNE).

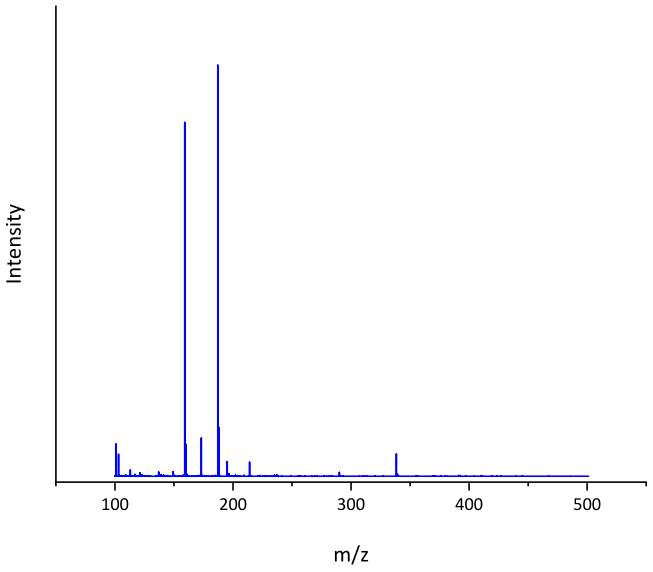

Fig. S9. Mass Spectra of ethyl nonanoate (ENE).

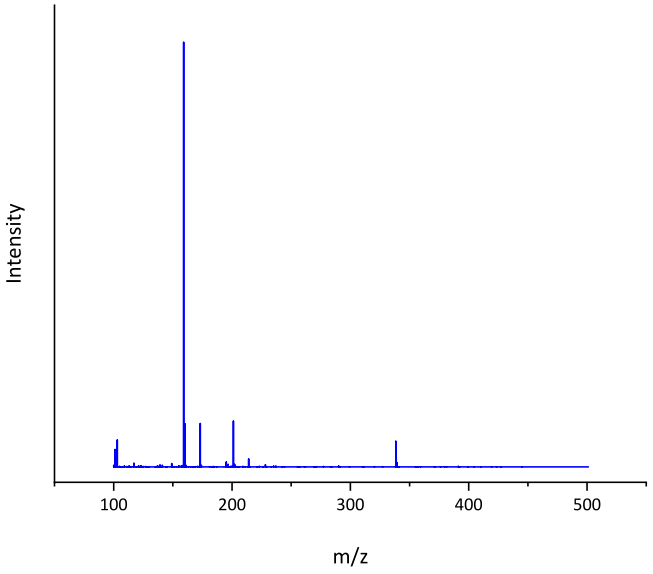

Fig. S10. Mass Spectra of propyl nonanoate (PNE).

Please cite this article as: Liu J., Molina E.R., Moiser N.S. Sustainable biokerosene from lipids using efficient ozone cracking. Biofuel Research Journal 46 (2025) 2412-2431. DOI: 10.18331/BRJ2025.12.2.4.

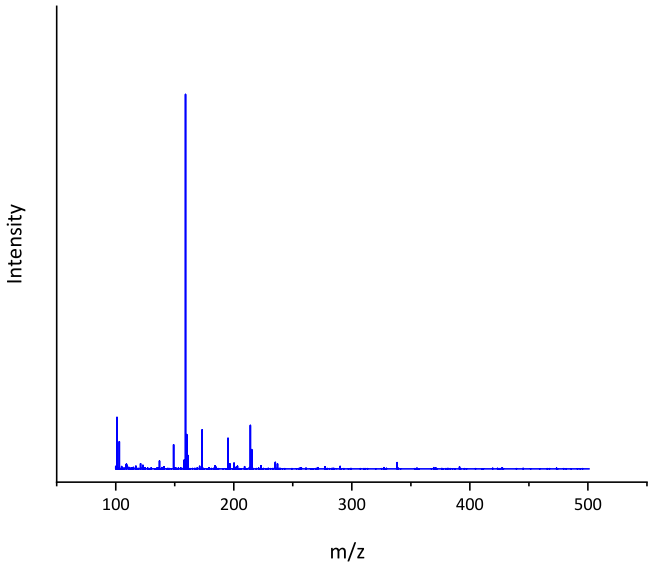

Fig. S11. Mass Spectra of butyl nonanoate (BNE).

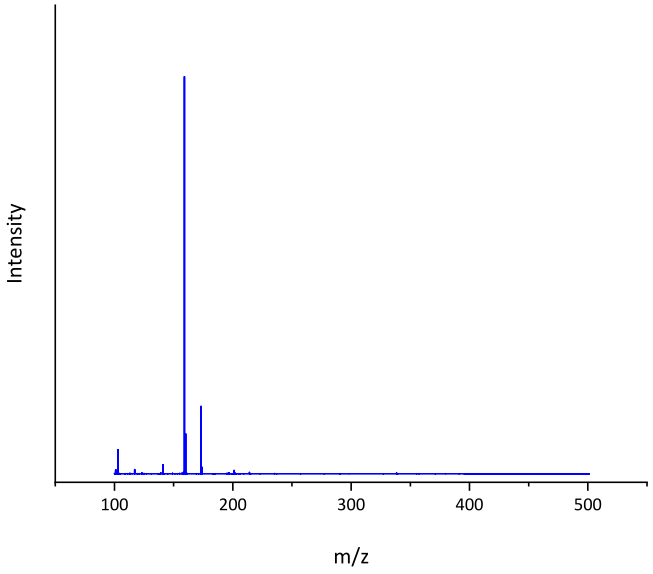

Fig. S12. Mass Spectra of isopropyl nonanoate (iPNE).

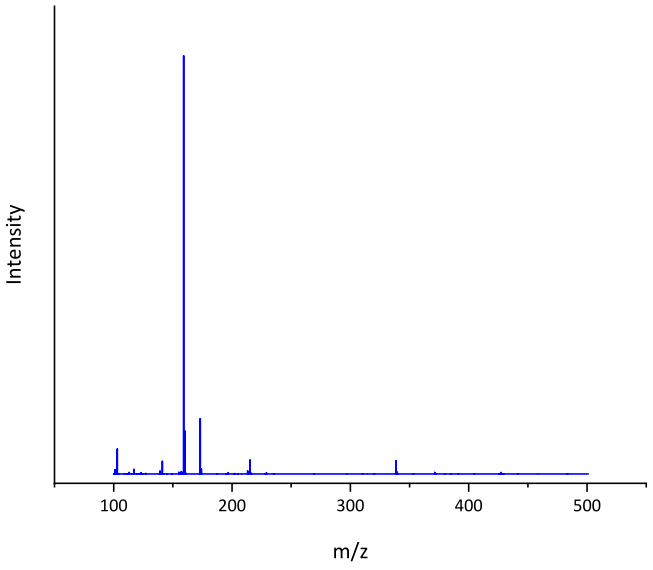

Fig. S13. Mass Spectra of isobutyl nonanoate (iBNE).

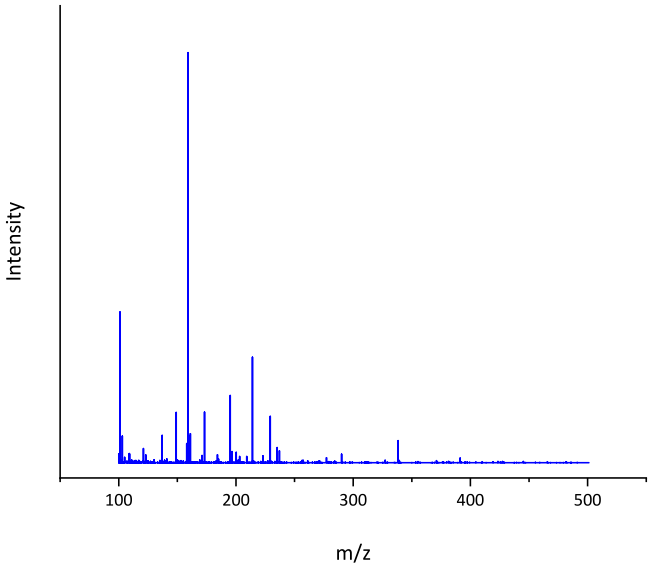

Fig. S14. Mass Spectra of isopentyl nonanoate (iPENE).

Please cite this article as: Liu J., Molina E.R., Moiser N.S. Sustainable biokerosene from lipids using efficient ozone cracking. Biofuel Research Journal 46 (2025) 2412-2431. DOI: 10.18331/BRJ2025.12.2.4.

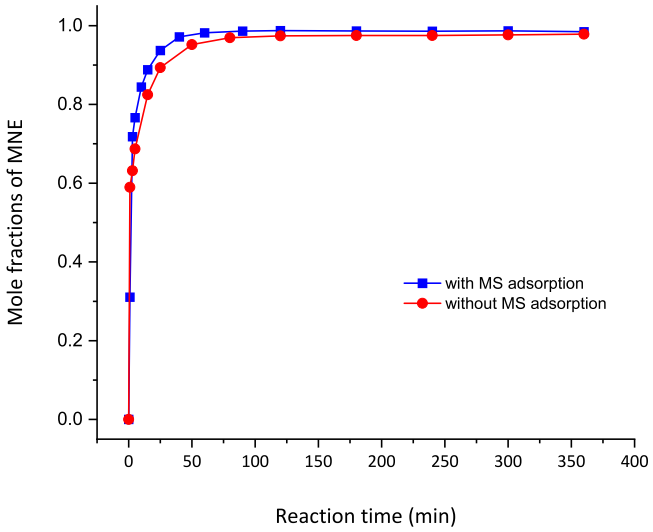

Fig. S15. Changes of mole fractions of MNE for reaction with MS adsorption and without MS adsorption.

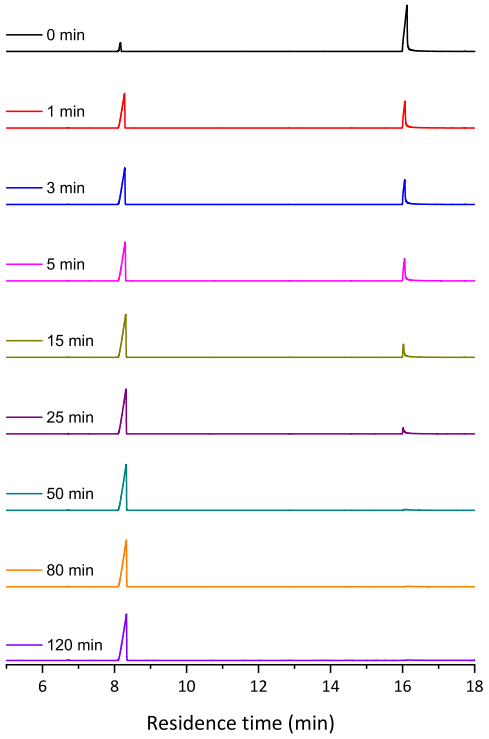

Fig. S16. Reaction process with molecular sieves adsorption for nonanoic acid and methanol solution monitoring by GC signal changes of nonanoic acid (residence time at 16.05 min) and MNE (residence time at 8.23 min) at various reaction times.

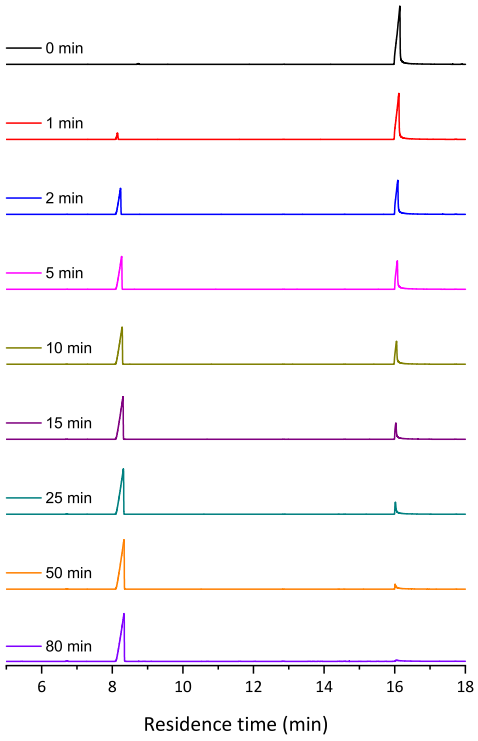

Fig. S17. Reaction process without molecular sieves adsorption for nonanoic acid and methanol solution monitoring by GC signal changes of nonanoic acid (residence time at 16.05 min) and MNE (residence time at 8.23 min) at various reaction times.

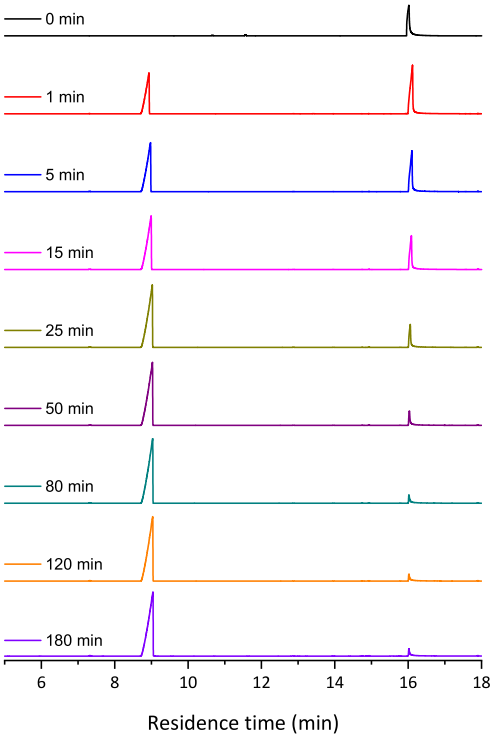

Fig. S18. Reaction process without molecular sieves adsorption for nonanoic acid and ethanol solution monitoring by GC signal changes of nonanoic acid (residence time at 16.05 min) and ENE (residence time at 8.92 min) at various reaction times.

Please cite this article as: Liu J., Molina E.R., Moiser N.S. Sustainable biokerosene from lipids using efficient ozone cracking. Biofuel Research Journal 46 (2025) 2412-2431. DOI: 10.18331/BRJ2025.12.2.4.

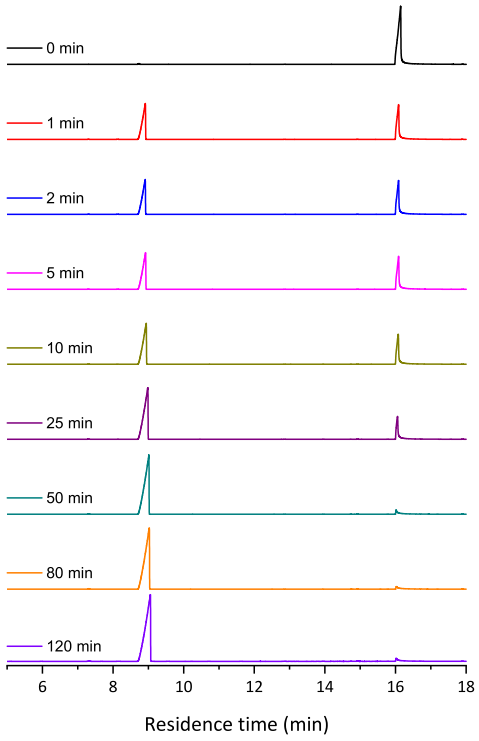

Fig. S19. Reaction process with molecular sieves adsorption for nonanoic acid and ethanol solution monitoring by GC signal changes of nonanoic acid (residence time at 16.05 min) and ENE (residence time at 8.92 min) at various reaction times.

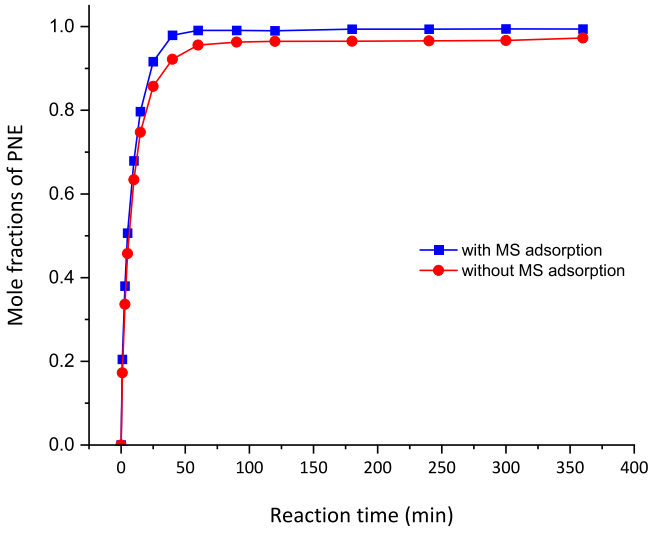

Fig. S20. Changes of mole fractions of PNE over time for reaction with MS adsorption and without MS adsorption.

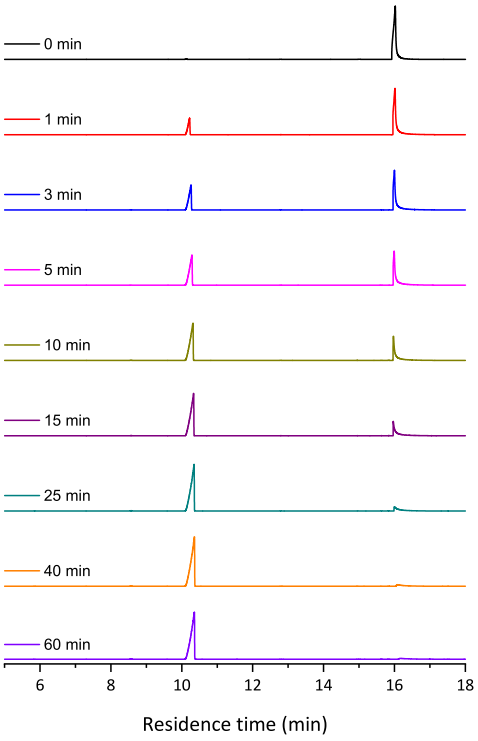

Fig. S21. Reaction process without molecular sieves adsorption for nonanoic acid and propanol solution monitoring by GC signal changes of nonanoic acid (residence time at 16.05 min) and PNE (residence time at 10.36 min) at various reaction times.

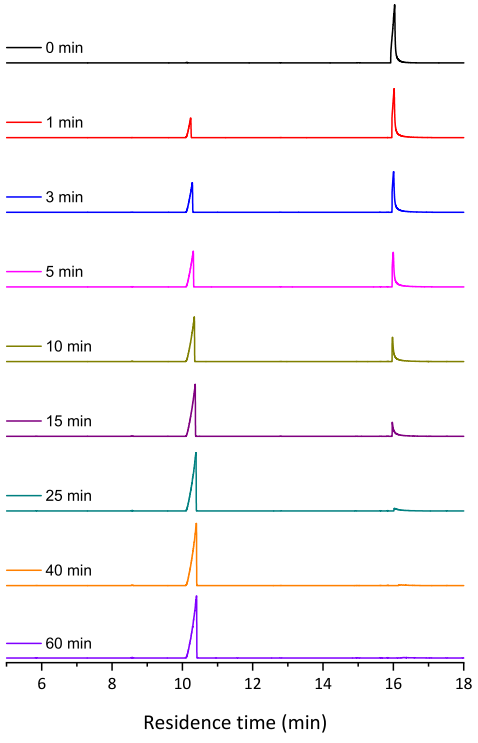

Fig. S22. Reaction process with molecular sieves adsorption for nonanoic acid and propanol solution monitoring by GC signal changes of nonanoic acid (residence time at 16.05 min) and PNE (residence time at 10.36 min) at various reaction times.

Please cite this article as: Liu J., Molina E.R., Moiser N.S. Sustainable biokerosene from lipids using efficient ozone cracking. Biofuel Research Journal 46 (2025) 2412-2431. DOI: 10.18331/BRJ2025.12.2.4.

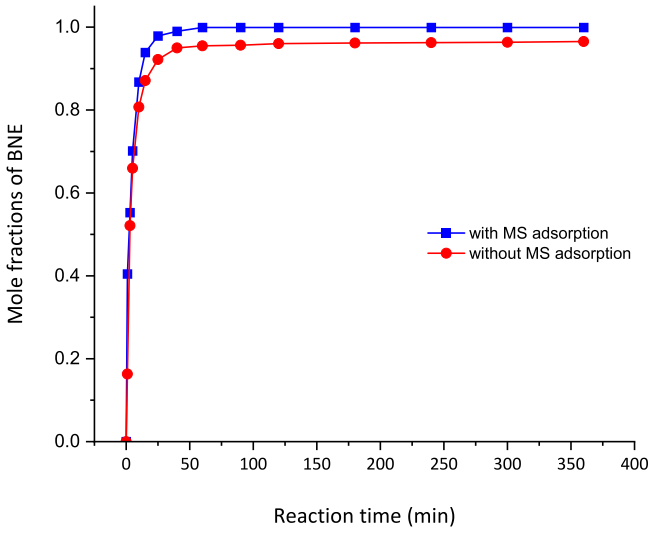

Fig. S23. Changes of mole fractions of BNE over time for reaction with MS adsorption and without MS adsorption.

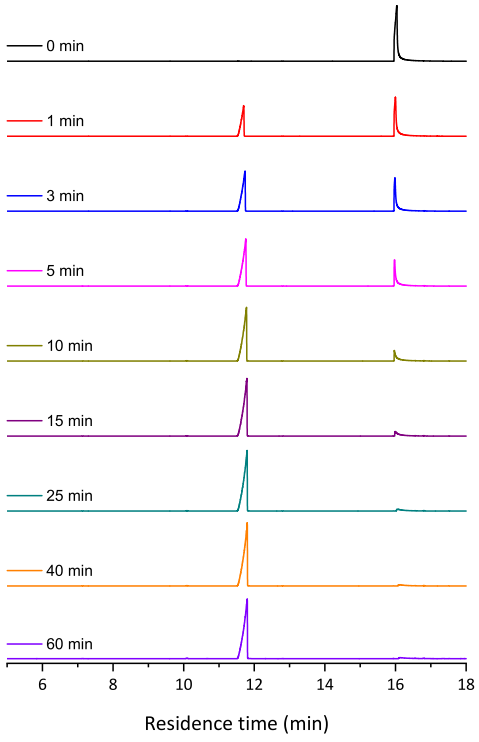

Fig. S24. Reaction process without molecular sieves adsorption for nonanoic acid and butanol solution monitoring by GC signal changes of nonanoic acid (residence time at 16.05 min) and BNE (residence time at 11.71 min) at various reaction times.

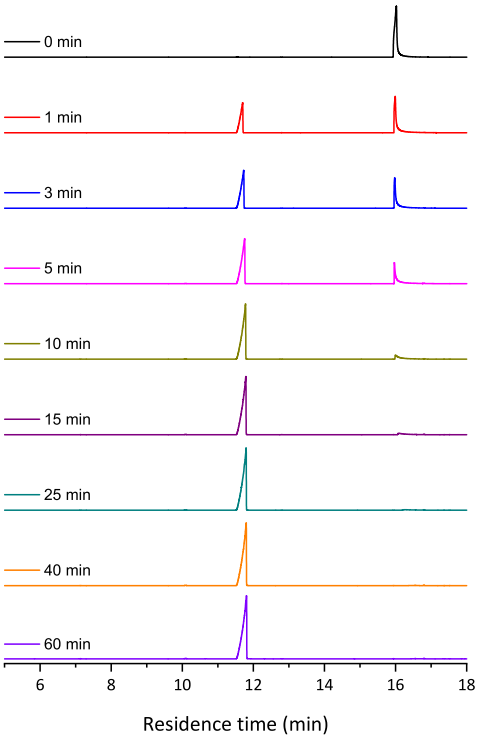

Fig. S25. Reaction process with molecular sieves adsorption for nonanoic acid and butanol solution monitoring by GC signal changes of nonanoic acid (residence time at 16.05 min) and BNE (residence time at 11.71 min) at various reaction times.

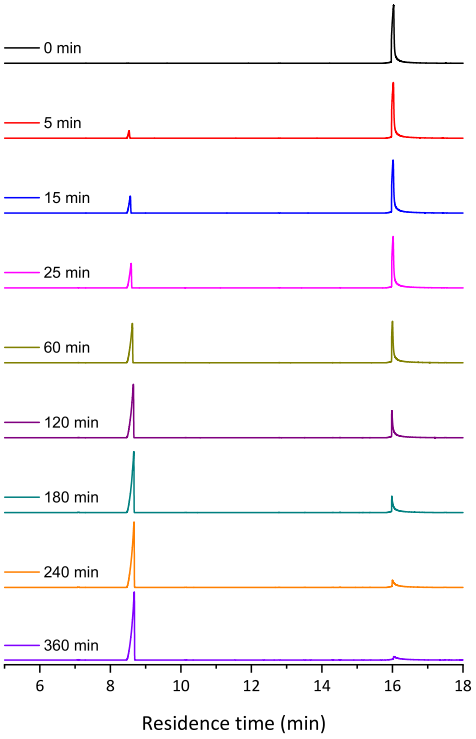

Fig. S26. Reaction process without molecular sieves adsorption for nonanoic acid and isopropyl solution monitoring by GC signal changes of nonanoic acid (residence time at 16.05 min) and iPNE (residence time at 8.68 min) at various reaction times.

Please cite this article as: Liu J., Molina E.R., Moiser N.S. Sustainable biokerosene from lipids using efficient ozone cracking. Biofuel Research Journal 46 (2025) 2412-2431. DOI: 10.18331/BRJ2025.12.2.4.

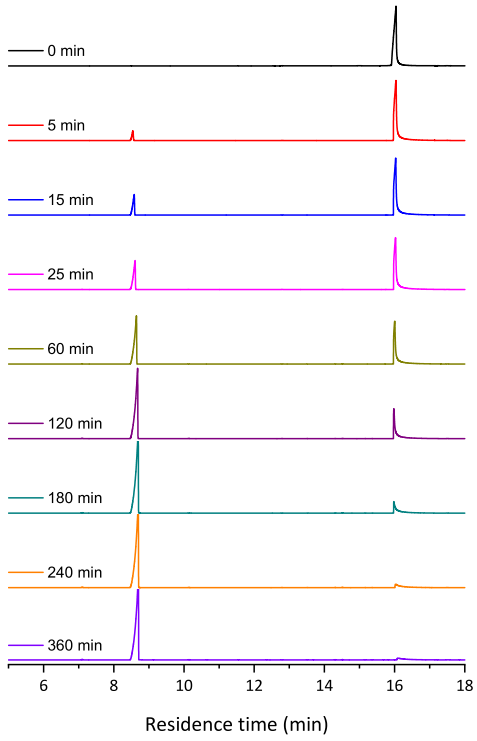

Fig. S27. Reaction process with molecular sieves adsorption for nonanoic acid and isopropyl solution monitoring by GC signal changes of nonanoic acid (residence time at 16.05 min) and iPNE (residence time at 8.68 min) at various reaction times.

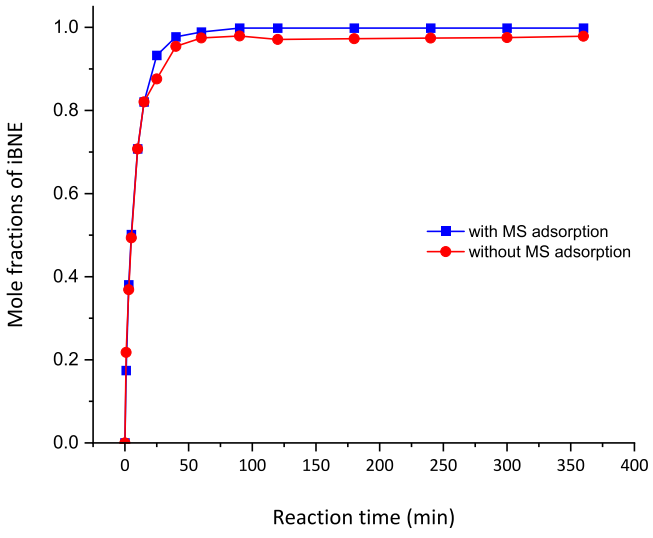

Fig. S28. Changes of mole fractions of iBNE over time for reaction with MS adsorption and without MS adsorption.

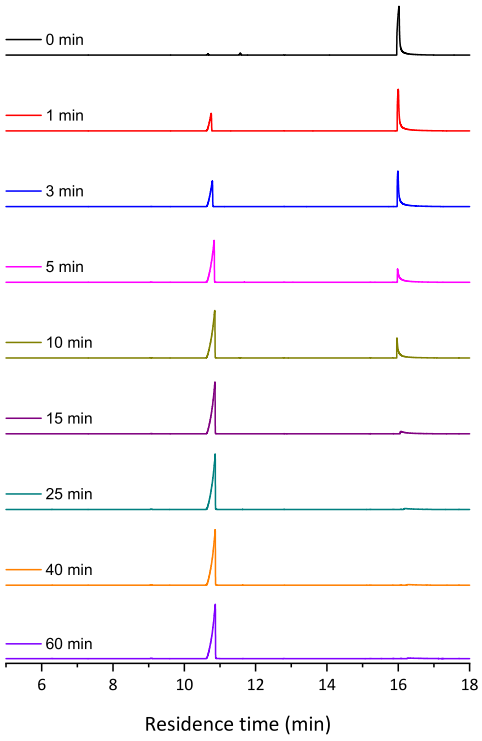

Fig. S29. Reaction process without molecular sieves adsorption for nonanoic acid and isobutanol solution monitoring by GC signal changes of nonanoic acid (residence time at 16.05 min) and iBNE (residence time at 10.79 min) at various reaction times.

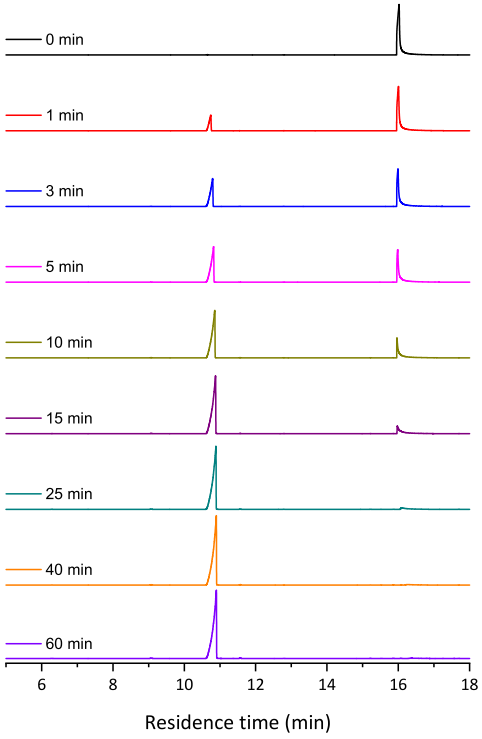

Fig. S30. Reaction process without molecular sieves adsorption for nonanoic acid and isobutanol solution monitoring by GC signal changes of nonanoic acid (residence time at 16.05 min) and iBNE (residence time at 10.79 min) at various reaction times.

Please cite this article as: Liu J., Molina E.R., Moiser N.S. Sustainable biokerosene from lipids using efficient ozone cracking. Biofuel Research Journal 46 (2025) 2412-2431. DOI: 10.18331/BRJ2025.12.2.4.

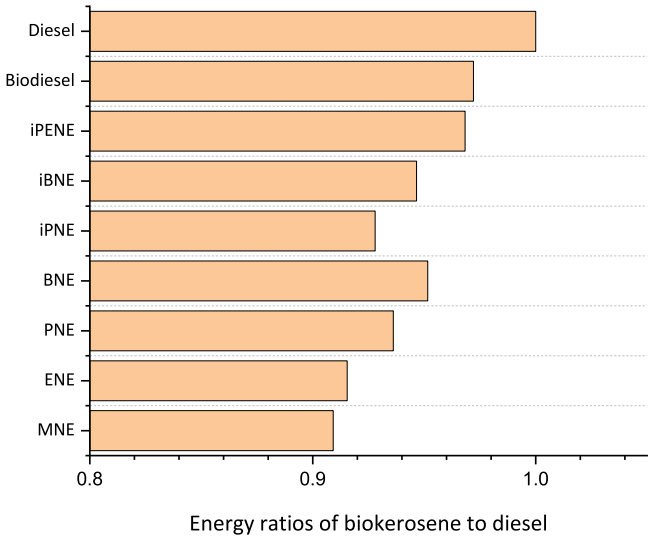

Fig. S31. Energy ratios of biokerosene to hydrocarbon diesel at the same tank size.

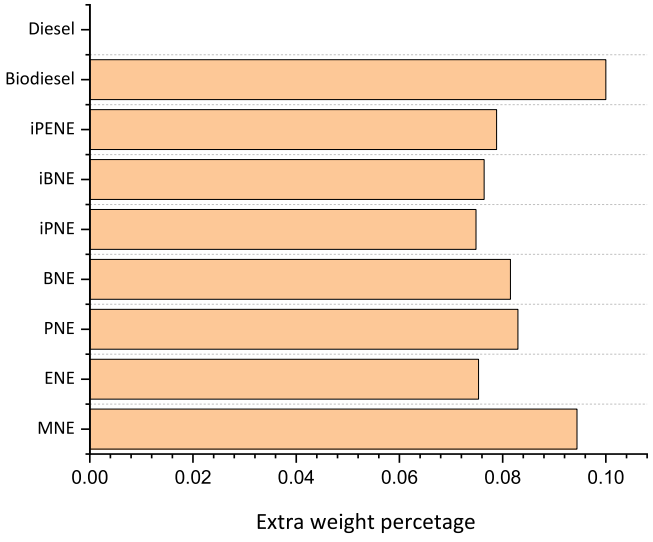

Fig. S32. Extra weight percentage of biokerosene over hydrocarbon diesel at the same tank size.

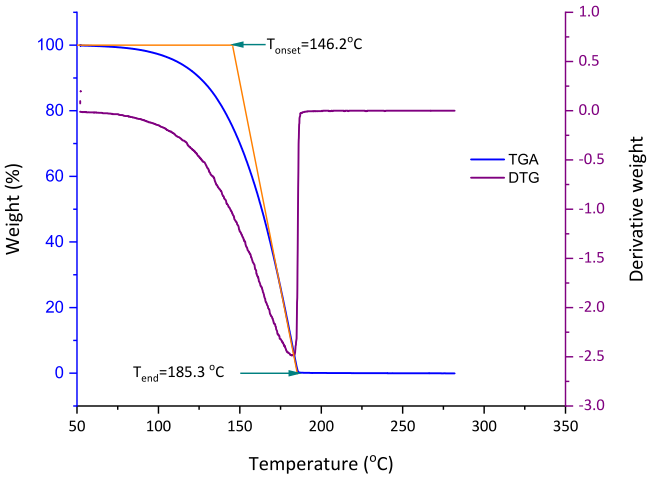

Fig. S33. TGA and DTG curves of MNE.

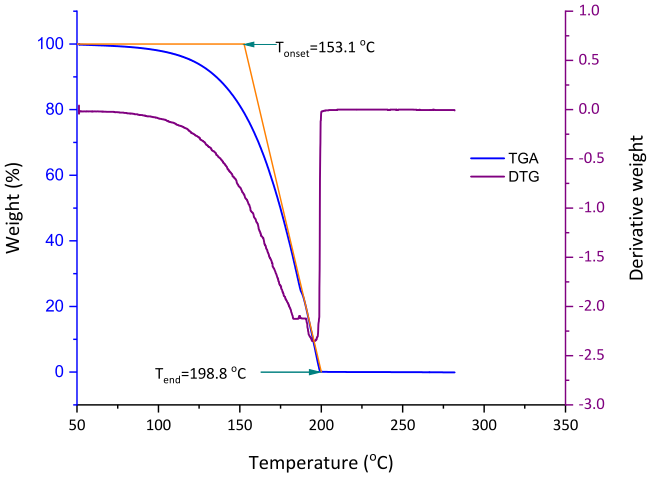

Fig. S34. TGA and DTG curves of ENE.

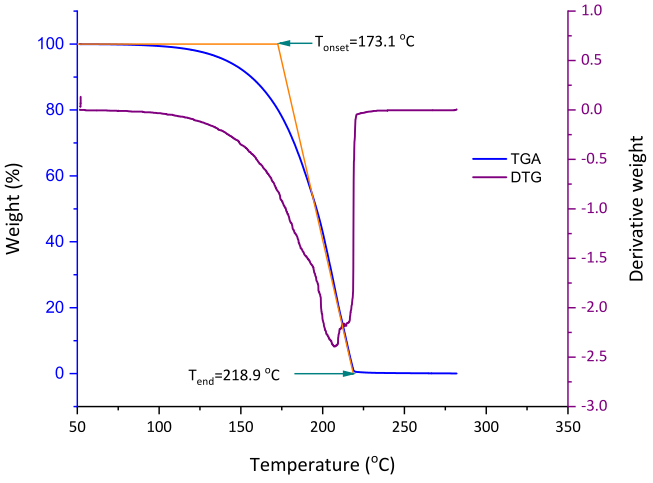

Fig. S35. TGA and DTG curves of PNE.

Please cite this article as: Liu J., Molina E.R., Moiser N.S. Sustainable biokerosene from lipids using efficient ozone cracking. Biofuel Research Journal 46 (2025) 2412-2431. DOI: 10.18331/BRJ2025.12.2.4.

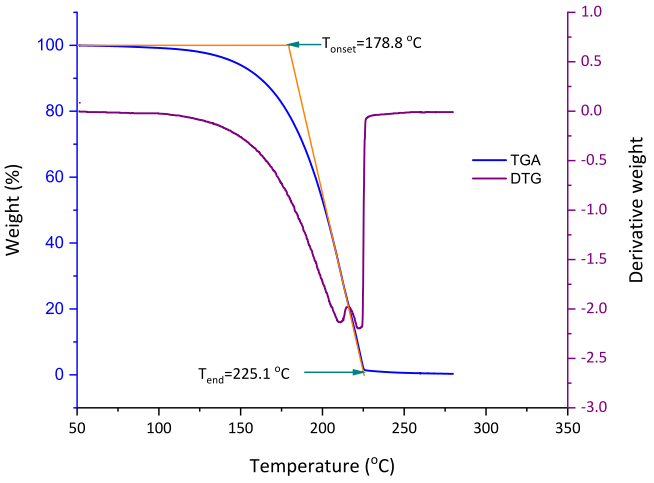

Fig. S36. TGA and DTG curves of BNE.

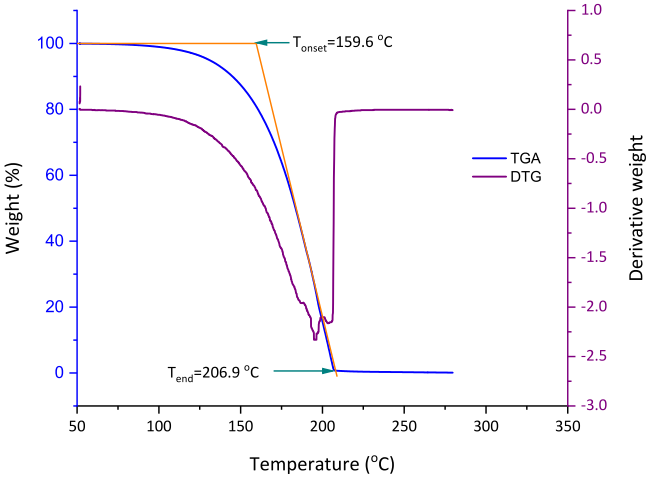

Fig. S37. TGA and DTG curves of iPNE.

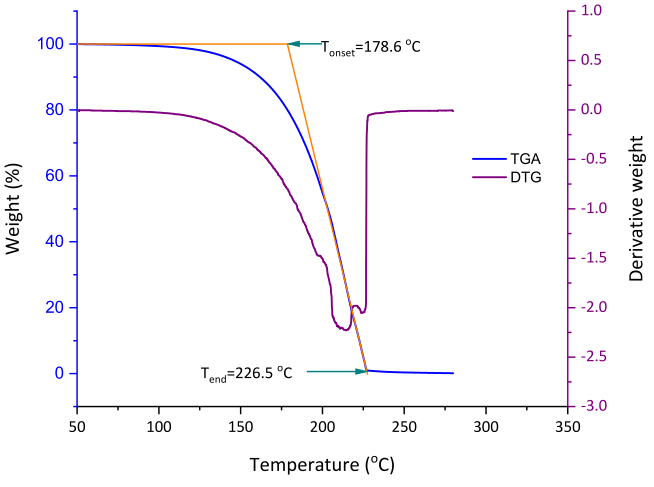

Fig. S38. TGA and DTG curves of iBNE.

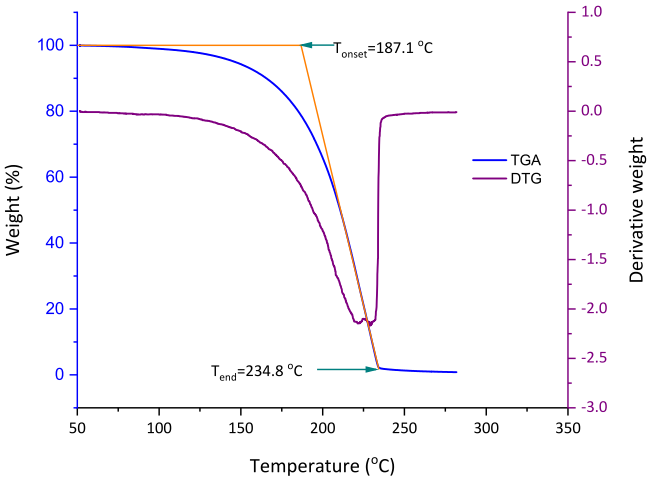

Fig. S39. TGA and DTG curves of iPENE.

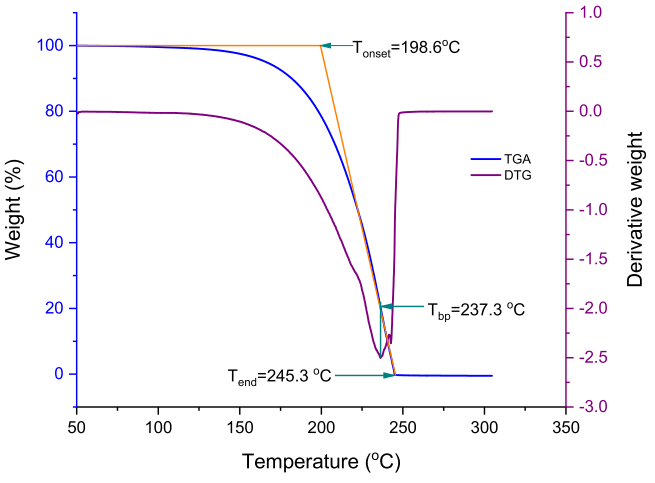

Fig. S40. TGA and DTG curves of nonoaic acid.

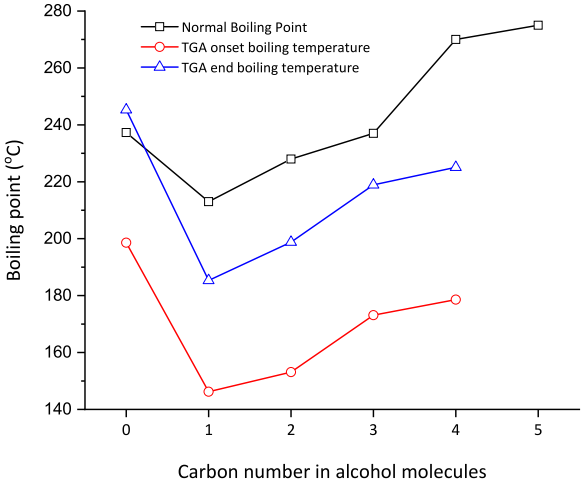

Fig. S41. Comparison of normal boiling points, TGA onset boiling temperature, and TGA end boiling temperature for nonanoates formed with n-alcohols (0 is the nonanoic acid).

Please cite this article as: Liu J., Molina E.R., Moiser N.S. Sustainable biokerosene from lipids using efficient ozone cracking. Biofuel Research Journal 46 (2025) 2412-2431. DOI: 10.18331/BRJ2025.12.2.4.

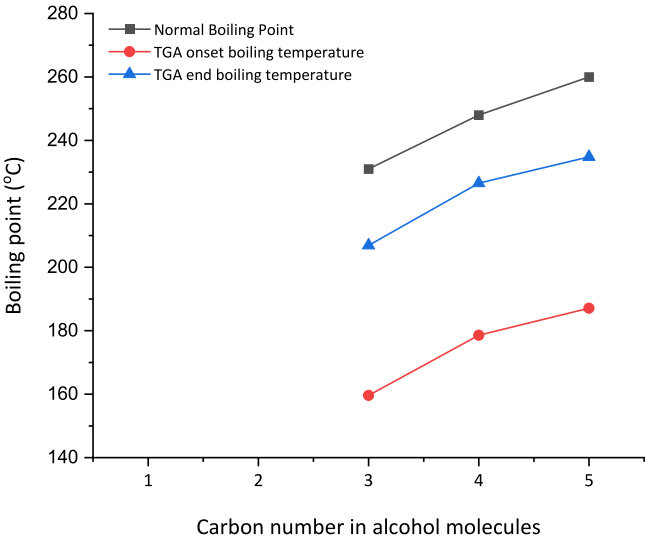

Fig. S42. Comparison of normal boiling points, TGA onset boiling temperature, and TGA end boiling temperature for nonanoates formed with iso-alcohols.

References

[1] Kurz R., Winkelmann B., Freund S., McBain M., Keith M., Zhang D., Cich S., Renzi P., Schmitt J. 2022. Transport and storage, in: Brun K., Allison T. (Eds.), Machinery and Energy Systems for the Hydrogen Economy. Elsevier.

[2] Liu, J., Ma, H., Liang, W., Yang, J., Sun, P., Wang, X., Wang, Y., Wang, P., 2022. Experimental investigation on combustion characteristics and influencing factors of PODE/methanol dual-fuel engine. Energy. 260, 125131.

[3] Liu, J., Tao, B.Y., Feng, H., Mosier, N.S., 2023. Efficient rapid fractionation of fatty acid methyl esters (FAMEs) through evaporative urea inclusion. J. Chem. Eng. 454, 140266.

[4] Weimar, N., 2020. Energy density and specific energy of battery. Sinovoltaics.com.

[5] Xue, C., Cheng, C., 2019. Butanol production by Clostridium. Advances in Bioenergy. Elsevier.

Please cite this article as: Liu J., Molina E.R., Moiser N.S. Sustainable biokerosene from lipids using efficient ozone cracking. Biofuel Research Journal 46 (2025) 2412-2431. DOI: 10.18331/BRJ2025.12.2.4.